

Article

Phase Diagram, Scalar-Pseudoscalar Meson Behavior and Restoration of Symmetries in (2 + 1) Polyakov-Nambu-Jona-Lasinio Model

Pedro Costa ^{*,†}  and Renan Pereira [†] 

Centro de Física da Universidade de Coimbra (CFisUC), Department of Physics, University of Coimbra, P-3004-516 Coimbra, Portugal; renan.pereira@student.fisica.uc.pt

* Correspondence: pcosta@uc.pt

† These authors contributed equally to this work.

Received: 14 March 2019; Accepted: 4 April 2019; Published: 8 April 2019



Abstract: We explore the phase diagram and the modification of mesonic observables in a hot and dense medium using the (2 + 1) Polyakov-Nambu-Jona-Lasinio model. We present the phase diagram in the (T, μ_B) -plane, with its isentropic trajectories, paying special attention to the chiral critical end point (CEP). Chiral and deconfinement transitions are examined. The modifications of mesonic observables in the medium are explored as a tool to analyze the effective restoration of chiral symmetry for different regions of the phase diagram. It is shown that the meson masses, namely that of the kaons, change abruptly near the CEP, which can be relevant for its experimental search.

Keywords: phase transition; chiral symmetry; restoration of symmetry

PACS: 11.10.Wx; 11.30.Rd; 14.40.Aq

1. Introduction

Since its creation in 1961 by Yoichiro Nambu and Giovanni Jona-Lasinio [1,2], the Nambu-Jona-Lasinio (NJL) model has been used in multiple applications. The NJL model is a pre-Quantum Chromodynamics (QCD) model that was introduced to describe the pion as a bound state of a nucleon and an antinucleon. Indeed, in its first version, the NJL model was formulated as an effective theory of nucleons and mesons, constructed from Dirac fermions that interact via four-fermion interactions with chiral symmetry, analogous with Cooper pairs in the Bardeen-Cooper-Schrieffer theory (BCS) theory of superconductivity (simultaneously and independently, the analogy between the four fermion masses and gaps in superconductors was also proposed by V. G. Vaks and A. I. Larkin [3]). The key idea was that the mass gap in the Dirac spectrum of the nucleon can be generated analogously with the energy gap of a superconductor in BCS theory. Later, the nucleon fields were replaced by quark fields (u , d and s) and it is still used to this day as an effective low-energy and model of QCD. The introduction of quark degrees of freedom, in the chiral limit (the bare quark mass is $m_i = 0$), and the description of hadrons were made by T. Eguchi and K. Kikkawa [4,5] and in a more realistic version with $m_i \neq 0$ by D. Ebert and M. Volkov [6–8].

The central point of the NJL model becomes the fact that its Lagrangian density contains the most important symmetries of QCD that are also observed in nature, namely chiral symmetry, which is fundamental to understand the physics of the lightest hadrons. The NJL model also embodies a spontaneous symmetry breaking mechanism. As matter of fact, within this approach, mesons can be interpreted as quark-antiquark excitations of the vacuum and baryons as bound states of quarks (solitons or quark-diquarks structures) [9].

Another relevant aspect is the fact that the interaction between quarks is assumed to be point-like (the gluon degrees of freedom are considered to be frozen into point-like quark-(anti-)quark vertices), attractive leading to a quark-antiquark pair condensation in the vacuum. However, the result of this point-like interaction is that the NJL model is not a renormalizable field theory and a regularization scheme must be specified to deal with the improper integrals that occur. Another well-known shortcoming of NJL-type models is the absence of gluons and the lack of the QCD property of color confinement, which implies that some care must be taken when applying the theory to high energies.

Over time, the model has undergone several improvements, a very important one was the introduction of a term simulating the $U_A(1)$ anomaly [10–12], which is known as the Kobayashi-Maskawa-'t Hooft (KMT) term [13–16]. This new KMT term is a six-fermion interaction that can be written in a determinantal form. It breaks the unwanted axial $U_A(1)$ symmetry of the four-quark NJL Lagrangian. Indeed, it is well known that in the chiral limit, i.e., $m_u = m_d = m_s = 0$, QCD has a $U(3)$ chiral symmetry. When this symmetry is spontaneously broken, it implies the existence of nine massless Goldstone bosons. However, in nature, only eight light pseudoscalar mesons exist: $\pi^0, \pi^+, \pi^-, K^+, K^-, K^0, \bar{K}^0$ and η . The Adler-Bell-Jackiw $U_A(1)$ anomaly solves this discrepancy, and the eventual ninth Goldstone boson, the η' , gets a mass (around 1 GeV) due to the fact that the density of topological charges in the QCD vacuum is nonzero [17,18]. Since the origin of the mass of the η' -meson is different from the masses of the other pseudoscalar mesons, this meson cannot be seen as the remnant of a Goldstone boson. Interestingly, the KMT term also induces a mixing between different quark flavors with very important consequences in the scalar and pseudoscalar mesons. We emphasize the following review works on this model [9,19–21].

Over the past decade, two major improvements of the NJL model took place: the introduction of eight-quark interactions with the purpose of stabilizing the asymmetric ground state of the model with four and six-quark 't Hooft interactions [22–24]; the introduction of the Polyakov loop effective field in order to consider characteristics of both the chiral symmetry breaking and the deconfinement. The latter resulted in the so-called Polyakov loop—Nambu-Jona-Lasinio (PNJL) model [25–27].

In the PNJL model, the Lagrangian contains static degrees of freedom that are introduced through an effective gluon potential in terms of the Polyakov loop [25–32]. This coupling of quarks to the Polyakov loop effectively induces the reduction of the weight of the quark degrees of freedom at low temperature. This is a consequence of the restoration of the \mathbb{Z}_{N_c} symmetry related with the color confinement. Indeed, in these new types of models, the Polyakov loop effective field is not a dynamical degree of freedom because the Lagrangian does not contain any dynamical term. The gluon dynamics are simply reduced to a chiral-point coupling between quarks, combined with a static background field representing the Polyakov loop [27].

One of the first big achievements of the NJL model was the study of meson properties at finite temperature and density, first in $SU(2)$ sector [33–35] then in the $(2 + 1)$ -flavors, where the role of strangeness was taken in consideration [11,36–44]. The chiral symmetry restoration through the point of view of the chiral partners has entered in the agenda. Indeed, experimentally, the manifestation of chiral symmetry would be the existence of parity doublets, that is, a multiplet of particles with the same mass and opposite parity for each multiplet of isospin (the so-called chiral partners) in the hadronic spectrum, a situation is not verified in nature. However, as the temperature increases, the chiral partners should have the same mass [45–47]. The same happens for increasing densities, even for different environment scenarios [47–50].

The study on the modification of the mesonic observables in the hot medium (used as a tool for understanding the restoration of chiral and axial symmetries) was extended to the $(2 + 1)$ -flavor PNJL model to infer the role of the Polyakov loop. It was concluded that the partial restoration of the chiral symmetry is faster in the PNJL model than in the NJL model [51]. The properties of the mesons in the PNJL were also studied in [48–50,52,53].

Interestingly, the NJL model has also been used to study mesons containing charmed quarks like D and B -mesons [54–57], in order to describe both the light and heavy quarks in one model. The same

mesons were studied within the PNJL model, with particular focus on the modification of the D -meson properties (masses and widths) in hot and dense matter. The purpose was to find the consequences of the possible non dropping of the D -meson masses in the medium for J/ψ suppression scenarios [58].

Another aspect where the NJL model (and its extensions) proved to be very useful was in the study of the possible phases of strongly-interacting matter. Since the first conjecture by N. Cabibbo and G. Parisi [59], the QCD phase diagram has been widely studied by both theoretical and experimental physicists (for a general review see [60]). In fact, in the hot and dense region of the phase diagram, the QCD phase structure is replete of rich details [61,62], namely the nature of the hadron matter-quark gluon plasma (QGP) transition and the possible existence of the QCD chiral critical endpoint (CEP), have been subject of remarkable theoretical and experimental efforts. In this region, QCD is non-perturbative, meaning that the set of theoretical tools available to study the phase transitions and meson behavior is limited. Some options on the table are lattice gauge theory applied to QCD (lattice QCD), Dyson-Schwinger equations and effective models. Lattice QCD is a first principles method however, at finite density, it suffers from the so-called sign problem, which renders the importance sampling needed in Monte Carlo simulations not appropriate [63]. Different methods are currently trying to fix, or circumvent, this issue like reweighting, Taylor expansions, considering an imaginary chemical potential and complex Langevin [63,64]. Dyson-Schwinger equations are a method based on the QCD effective action [65,66]. This method generates an infinite tour of integro-differential equations for the Green's function of the theory that need to be truncated at some order. Making a proper truncation is not a simple task and several techniques have been developed and applied throughout the years [67]. The use of effective models of QCD allows access to the entire phase diagram rooting the model to experimental or lattice QCD data. The main disadvantage of using effective models is that they are not derived from first principles; one should only study the model inside its range of applicability.

One interesting and very timely topic of the phase diagram of strong interactions, is the possible existence and location of the chiral CEP. The CEP is a conjectured second order phase transition point in the $(T - \mu_B(\rho_B))$ -plane (belonging to the three-dimensional Ising universality class), which separates the crossover transition at zero density predicted by lattice QCD calculations [68,69] and a possible first-order phase transition in the cold and dense region of the diagram. Old lattice results [70], Dyson-Schwinger calculations [71,72] and several models predict its existence but this remains a matter of debate.

Experimentally, a major goal of heavy ion collision (HIC) experiments is not only to map the the QCD phase boundaries but also settle the question about the existence of the elusive CEP. Indeed, the search for the CEP is already being carried out in several facilities such as the Relativistic Heavy Ion Collider (RHIC) (STAR Collaboration) at Brookhaven National Laboratory [73–75] and in the Super Proton Synchrotron (SPS) (NA61/SHINE Collaboration) at CERN [76,77]; Future facilities like the J-PARC Heavy Ion Project at Japan Proton Accelerator Research Complex (J-PARC) [78], the Facility for Antiproton and Ion Research (FAIR) at GSI Helmholtzzentrum für Schwerionenforschung [79] and the Nuclotron-based Ion Collider fAcility (NICA) at Joint Institute for Nuclear Research [80], have planned experiments to its search (a review on the experimental search of the CEP can be found in Ref. [81]).

One of the first suggestions for a first-order phase transition in the framework of the standard SU(2) NJL model was made in [82] and the study of the phase diagram in the same version of the model at finite temperature and density was presented in [83]. Also in the framework of the standard SU(2) NJL model, the calculation of the hadronization cross section in a quark plasma at finite temperatures and densities was done in Reference [84]. After that, several studies have addressed the peculiarities of the different versions of the model, namely the SU(2) [85–87] and $(2 + 1)$ -flavors [88–90]. The PNJL model brings with it some changes relative to the NJL model, in both SU(2) and $(2 + 1)$ -flavor versions, particularly concerning to a higher temperature for the position of the CEP and also a larger size of the critical region [91–95].

The applications of NJL and PNJL models are indeed very wide, see for example their usefulness in the study of neutron stars [96–102] or the influence of strong magnetic fields [103–109].

In the present work, we will consider the PNJL model to explore the QCD phase diagram and the in-medium behavior of scalar and pseudoscalar mesons, especially the hot and dense regions near the chiral transition.

This paper is organized as follows. In Section 2, we present the PNJL model used throughout the work to study the phase diagram of QCD and the behavior of scalar and pseudoscalar mesons. In Section 3, we present the phase diagram and analyze some features of both the chiral and deconfinement transitions. Special attention is given to the isentropic trajectories near the CEP. In Section 4, we study the behavior of scalar and pseudoscalar mesons in six different paths that cross the phase diagram: zero density, zero temperature, crossover, CEP, first-order and a path following an isentropic line. Finally, we present the concluding remarks in Section 5.

2. Model and Formalism

2.1. The PNJL Model

The $SU_f(3)$ Nambu–Jona-Lasinio model, including the 't Hooft interaction (the inclusion of this term is not only important to correctly reproduce the symmetries of QCD, but also allows to reproduce the correct mass split between the η and η' mesons in $SU_f(3)$ [13,19]), which explicitly breaks $U_A(1)$, is defined via the following Lagrangian density:

$$\mathcal{L}_{\text{NJL}} = \bar{\psi}(i\partial - \hat{m})\psi + \frac{g_S}{2} \sum_{a=0}^8 \left[(\bar{\psi}\lambda^a\psi)^2 + (\bar{\psi}i\gamma^5\lambda^a\psi)^2 \right] + g_D [\det(\bar{\psi}(1 + \gamma_5)\psi) + \det(\bar{\psi}(1 - \gamma_5)\psi)]. \quad (1)$$

Here, the quark field ψ , is a 3-component vector in flavor space, where each component is a Dirac spinor, $\hat{m} = \text{diag}(m_u, m_d, m_s)$ is the quark current mass matrix, diagonal in flavor space. The matrices λ^a with $a = 1, \dots, 8$, are the Gell-Mann matrices and $\lambda^0 = \sqrt{2/3}\mathbb{1}_{3 \times 3}$.

Following [51], the bosonization procedure can be easily carried out after the 't Hooft six-quark interaction is reduced to a four-quark interaction. One gets:

$$\mathcal{L}_{\text{eff}} = \bar{\psi}(i\partial - \hat{m})\psi + \frac{1}{2}S_{ab} [(\bar{\psi}\lambda^a\psi)(\bar{\psi}\lambda^b\psi)] + \frac{1}{2}P_{ab} [(\bar{\psi}i\gamma_5\lambda^a\psi)(\bar{\psi}i\gamma_5\lambda^b\psi)], \quad (2)$$

where the projectors S_{ab}, P_{ab} are given by

$$S_{ab} = g_S\delta_{ab} + g_D D_{abc} \langle \bar{q}\lambda^c q \rangle, \quad (3)$$

$$P_{ab} = g_S\delta_{ab} - g_D D_{abc} \langle \bar{q}\lambda^c q \rangle. \quad (4)$$

The constants D_{abc} coincide with the $SU_f(3)$ structure constants for $a, b, c = (1, 2, \dots, 8)$, while $D_{0ab} = -\frac{1}{\sqrt{6}}\delta_{ab}$ and $D_{000} = \sqrt{\frac{2}{3}}$. The quark fields can then be integrated out using the Hubbard-Stratonovich transformation.

The main shortcoming of the NJL model as an effective model of QCD is its inability to describe confinement physics. To remedy this situation and study the deconfinement transition, the Polyakov-NJL model was introduced by K. Fukushima [25], by coupling the NJL model to an order parameter that describes the $Z(N_c)$ symmetry breaking: the Polyakov loop.

One important global symmetry of QCD is the center symmetry of $SU(N_c)$, the $Z(N_c)$ symmetry. The breaking of this symmetry is associated to the deconfinement transition: $Z(N_c)$ is respected in the confined phase and broken in the deconfined phase. When considering pure glue theory at finite temperature, the boundary conditions of QCD are respected by the $Z(N_c)$ symmetry.

An order parameter for the possible $Z(N_c)$ symmetry breaking can be defined using the thermal Wilson line $L(\mathbf{x})$,

$$L(\mathbf{x}) = \mathcal{P} \exp \left[i \int_0^\beta d\tau A_4(\tau, \mathbf{x}) \right]. \quad (5)$$

\mathcal{P} is the path ordering operator and A_4 the gluon field in the time direction,

$$A_4 = ig \mathcal{A}_\mu^a \frac{\lambda_a^\mu}{2} \delta_0^\mu, \quad a = 1, \dots, N_c^2 - 1 \quad (6)$$

$$= iA_0, \quad A_0 = g \mathcal{A}_\mu^a \frac{\lambda_a^\mu}{2} \delta_0^\mu. \quad (7)$$

Here, \mathcal{A}_μ^a is the gluon field of color index a . The Polyakov loop Φ can be defined as the trace over color of the thermal Wilson line:

$$\Phi = \frac{1}{N_c} \text{tr}_c L(\mathbf{x}). \quad (8)$$

In the confined phase $\Phi \rightarrow 0$ while in the deconfined phase, $\Phi \rightarrow 1$.

The NJL model can be minimally coupled to the gluon field in the temporal direction, through the introduction of the covariant derivative:

$$\partial_\mu \rightarrow D_\mu = \partial_\mu - A_4^0 \delta_\mu^0. \quad (9)$$

One has also to add to the Lagrangian density the effective Polyakov-loop potential, $\mathcal{U}(\Phi, \bar{\Phi}; T)$, which represents the effective glue potential at finite temperature.

The ansatz for the Polyakov loop effective potential can be written in terms of the order parameter, using the Ginzburg-Landau theory of phase transitions. The potential has to respect the $Z(N_c)$ symmetry and to reproduce its spontaneous breaking at some high temperature. There are several potentials in the literature that fulfill these properties, e.g., [26,110,111]. We choose to adopt the one proposed in Reference [25,110]:

$$\frac{\mathcal{U}(\Phi, \bar{\Phi}; T)}{T^4} = -\frac{1}{2} a(T) \bar{\Phi} \Phi + b(T) \ln [X(\Phi, \bar{\Phi})], \quad (10)$$

with the T -dependent parameters [110],

$$a(T) = a_0 + a_1 \left(\frac{T_0}{T} \right) + a_2 \left(\frac{T_0}{T} \right)^2, \quad (11)$$

$$b(T) = b_3 \left(\frac{T_0}{T} \right)^3, \quad (12)$$

and where the argument in the logarithm is written as:

$$X(\Phi, \bar{\Phi}) = 1 - 6\Phi\bar{\Phi} + 4(\Phi^3 + \bar{\Phi}^3) - 3(\Phi\bar{\Phi})^2. \quad (13)$$

The parameters T_0, a_0, a_1, a_2 and a_3 are fixed by reproducing lattice QCD results at $\mu = 0$ [112–114]. A commonly used set is:

$$T_0 = 270 \quad (\text{in the pure gauge sector}),$$

$$a_0 = 3.51, \quad a_1 = -2.47,$$

$$a_2 = 15.2, \quad a_3 = -1.75.$$

To study the effects of finite density one can add to the Lagrangian density the term $\bar{\psi}\gamma^0\hat{\mu}\psi$, where $\hat{\mu} = \text{diag}(\mu_u, \mu_d, \mu_s)$. If considering the A_4 as a constant background mean field, it can be absorbed in the definition of the chemical potential, $\hat{\mu} \rightarrow \hat{\mu} - iA_4 = \tilde{\mu}$. The main effect of A_4 in the effective chemical potential is to change the distribution functions for particles and antiparticles, as shown in Reference [27].

In the present work, temperature and finite density effects will be introduced through the Matsubara formalism, which can be translated in the usual substitution, $p_0 \rightarrow i\omega_n + \hat{\mu}$:

$$\int \frac{d^4p}{(2\pi)^4} \rightarrow \frac{1}{-i\beta} \int \frac{d^3p}{(2\pi)^3} \sum_n. \tag{14}$$

where $\beta = 1/T$ and the sum is made over the Matsubara frequencies, ω_n .

2.2. Gap Equations

Considering the mean field approximation, the effective quark masses (the gap equations) can be derive from Equation (2) (see Reference [19]). One gets:

$$M_i = m_i - 2g_s \langle \bar{q}_i q_i \rangle - 2g_D \langle \bar{q}_j q_j \rangle \langle \bar{q}_k q_k \rangle, \tag{15}$$

where the quark condensates $\langle \bar{q}_i q_i \rangle$, with $i, j, k = u, d, s$, in cyclic order.

The $SU_f(3)$ PNJL grand canonical potential is:

$$\begin{aligned} \Omega = \mathcal{U}(\Phi, \bar{\Phi}; T) + g_s \sum_{i=u,d,s} \langle \bar{q}_i q_i \rangle^2 + 4g_D \langle \bar{q}_u q_u \rangle \langle \bar{q}_d q_d \rangle \langle \bar{q}_s q_s \rangle - 2N_c \sum_{i=u,d,s} \int \frac{d^3p}{(2\pi)^3} E_i \\ - 2 \sum_{i=u,d,s} \int \frac{d^3p}{(2\pi)^3} [\mathcal{F}(\mathbf{p}, T, \mu_i) + \mathcal{F}^*(\mathbf{p}, T, \mu_i)]. \end{aligned} \tag{16}$$

Here, E_i is the quasiparticle energy for the quark i : $E_i = \sqrt{\mathbf{p}^2 + M_i^2}$ and the thermal functions \mathcal{F} and \mathcal{F}^* are defined as:

$$\mathcal{F}(\mathbf{p}, T, \mu_i) = T \ln \left[1 + e^{-3(E_i - \mu_i)/T} + N_c \bar{\Phi} e^{-(E_i - \mu_i)/T} + N_c \Phi e^{-2(E_i - \mu_i)/T} \right], \tag{17}$$

$$\mathcal{F}^*(\mathbf{p}, T, \mu_i) = T \ln \left[1 + e^{-3(E_i + \mu_i)/T} + N_c \Phi e^{-(E_i + \mu_i)/T} + N_c \bar{\Phi} e^{-2(E_i + \mu_i)/T} \right], \tag{18}$$

To obtain the mean field equations, we apply the thermodynamic consistency relations, i.e., calculate the minima of the thermodynamical potential density, Equation (16), with respect to $\langle \bar{q}_i q_i \rangle$ ($i = u, d, s$), Φ , and $\bar{\Phi}$:

$$\frac{\partial \Omega}{\partial \langle \bar{q}_i q_i \rangle} = \frac{\partial \Omega}{\partial \Phi} = \frac{\partial \Omega}{\partial \bar{\Phi}} = 0, \quad i = u, d, s. \tag{19}$$

These relations define the value of the i -flavor quark condensate:

$$\langle \bar{q}_i q_i \rangle = -i \text{tr} [S_i(q)] = -2 N_c \int \frac{d^3p}{(2\pi)^3} \frac{M_i}{E_i} (1 - v_i - \bar{v}_i). \tag{20}$$

Here, $S_i(q)$ is the quark propagator of flavor i , v_i and \bar{v}_i are the particle and antiparticle occupation numbers in the PNJL model, defined as:

$$v_i = \frac{\frac{3}{N_c} e^{-3(E_i-\mu_i)/T} + \bar{\Phi} e^{-(E_i-\mu_i)/T} + 2\Phi e^{-2(E_i-\mu_i)/T}}{1 + e^{-3(E_i-\mu_i)/T} + N_c \bar{\Phi} e^{-(E_i-\mu_i)/T} + N_c \Phi e^{-2(E_i-\mu_i)/T}}, \tag{21}$$

$$\bar{v}_i = \frac{\frac{3}{N_c} e^{-3(E_i+\mu_i)/T} + \Phi e^{-(E_i+\mu_i)/T} + 2\bar{\Phi} e^{-2(E_i+\mu_i)/T}}{1 + e^{-3(E_i+\mu_i)/T} + N_c \Phi e^{-(E_i+\mu_i)/T} + N_c \bar{\Phi} e^{-2(E_i+\mu_i)/T}}. \tag{22}$$

The gap equations for the Polyakov loop fields Φ and $\bar{\Phi}$ are:

$$-\frac{1}{2} a(T) \bar{\Phi} - \frac{6b(T) (\bar{\Phi} - 2\Phi^2 + \bar{\Phi}^2 \Phi)}{X(\Phi, \bar{\Phi})} = \frac{2N_c}{T^3} \sum_{i=u,d,s} \int \frac{d^3p}{(2\pi)^3} \left[\frac{e^{-(E_i+\mu_i)/T}}{e^{\mathcal{F}^*(p,T,\mu_i)/T}} + \frac{e^{-2(E_i-\mu_i)/T}}{e^{\mathcal{F}(p,T,\mu_i)/T}} \right], \tag{23}$$

$$-\frac{1}{2} a(T) \Phi - \frac{6b(T) (\Phi - 2\bar{\Phi}^2 + \bar{\Phi} \Phi^2)}{X(\Phi, \bar{\Phi})} = \frac{2N_c}{T^3} \sum_{i=u,d,s} \int \frac{d^3p}{(2\pi)^3} \left[\frac{e^{-(E_i-\mu_i)/T}}{e^{\mathcal{F}(p,T,\mu_i)/T}} + \frac{e^{-2(E_i+\mu_i)/T}}{e^{\mathcal{F}^*(p,T,\mu_i)/T}} \right]. \tag{24}$$

In the $T = 0$ limit, the PNJL grand canonical potential is reduced to the usual NJL model. Indeed, in this limit, the Polyakov loop potential and the thermal function \mathcal{F}^* vanish while the function \mathcal{F} becomes a step-function. For more details, see the Appendix B. We draw attention to the fact that this feature is a consequence of the definition of the Polyakov loop potential in Equation (10). Actually, one can try to build a different Polyakov loop potential that does not vanish in the $T \rightarrow 0$ limit, by including for example, an explicit dependence in the chemical potential. Of course, such a modified potential would have to respect the $Z(N_c)$ of QCD, as well as, reproduce lattice observables.

2.3. Pseudoscalar and Scalar Meson Nonets

To study the meson mass spectrum and decays, we need to calculate the meson propagators. Following the same procedure outlined in detail in Reference [45,51], we expand the effective action to second order in the meson fields, yielding the following meson propagator:

$$D_{ab}^M(q) = \frac{1}{M_{ab}^{-1} - \Pi_{ab}^M(q)}. \tag{25}$$

Here, M_{ab} are the so-called projectors which, for scalar mesons are S_{ab} and for pseudoscalar mesons P_{ab} , defined in Equations (3) and (4). The polarization operator for the meson channel M , is:

$$\Pi_{ab}^M(q) = iN_c \int \frac{d^4p}{(2\pi)^4} \text{tr} \left[S_a(p) \Gamma_a^M S_b(p+q) \Gamma_b^M \right]. \tag{26}$$

The trace has to be made over flavor and Dirac spaces and $\Gamma_a^M = \lambda^a \otimes \Gamma^M$, where $\Gamma^M = \{1, i\gamma_5\}$. The explicit expression is presented in the Appendix A. As already stated, the introduction of the Polyakov loop is made in the quark propagator, $S_i(q)$, by the use of the modified Fermi functions, defined in Equations (21) and (22).

The calculation of the masses of the scalar and pseudoscalar mesons is done from the zeros of the inverse meson propagators in the rest frame, i.e.,

$$1 - M_{ab} \Pi_{ab}^M \left(M_M - i \frac{\Gamma_M}{2}, \mathbf{q} = \mathbf{0} \right) = 0. \tag{27}$$

Here, M_M and Γ_M are the mass and decay width of the meson channel M . The Mott dissociation is commonly identified by mass poles for mesons becoming complex: the real part being the “mass”, M_M , of the resonance; and the imaginary part being related to a finite width, Γ_M , due to its decay into the quark constituents (reflecting the fact that the NJL model does not confine the quarks). These two quantities are extracted from the zeroes of the complete real and imaginary components of Equation (27)

that can be written in the form of a system of two coupled equations. Usually, different approaches can also be used to compute M_M and Γ_M . In [95], the meson masses were calculated by supposing that the pole is near the real axis and the imaginary part of the solution in the argument of Equation (A3) of the Appendix A is neglected. In [47,51,115] only the Γ_M^2 contribution coming from $(M_M - i\Gamma_M/2)$ was neglected.

The quark-meson coupling constants are given by the residue at the poles of the propagators defined in Equation (25). It yields:

$$g_{M\bar{q}q}^{-2} = -\frac{1}{2M} \frac{\partial}{\partial q_0} \left[\Pi_{ab}^M(q_0) \right]_{q_0=M_M}, \quad (28)$$

where M_M is the mass of the bound state containing quark flavors a, b .

To calculate the masses of the η and η' mesons, we consider the basis of $\pi^0 - \eta - \eta'$ system (for more details see [116]). In the case where the π^0 is decoupled (this happens if $\langle \bar{q}_u q_u \rangle = \langle \bar{q}_d q_d \rangle$) from the $\eta - \eta'$, the following inverse propagators can be defined:

$$D_\eta^{-1}(q) = (A + C) - \sqrt{(C - A)^2 + 4B^2} \quad (29)$$

$$D_{\eta'}^{-1}(q) = (A + C) + \sqrt{(C - A)^2 + 4B^2} \quad (30)$$

with $A = P_{88} - \Delta \Pi_{00}^P(q)$, $C = P_{00} - \Delta \Pi_{88}^P(q)$, $B = -(P_{08} + \Delta \Pi_{08}^P(q))$ and $\Delta = P_{00}P_{88} - P_{08}^2$. Here, P_{ab} is defined in Equation (4).

In the rest frame, $D_\eta^{-1}(q_0 = M_\eta, \mathbf{q} = 0) = 0$, $D_{\eta'}^{-1}(q_0 = M_{\eta'}, \mathbf{q} = 0) = 0$. The mixing $\eta - \eta'$ pseudoscalar angle θ_P , is given by:

$$\tan 2\theta_P = \frac{2B}{A - C}. \quad (31)$$

Turning now to the scalar mesons σ and f_0 , the approach is identical to the one followed above. The propagators for these mesons and scalar angle θ_S , are identical to the ones in Equations (29)–(31). However, A , B and C are obtained by substituting $P_{ab} \rightarrow S_{ab}$ and $\Pi_{ab}^P(q) \rightarrow \Pi_{ab}^S(q)$.

2.4. Thermodynamics

Thermodynamic quantities are of great importance. Some of these quantities can be compared with the results that have become accessible in first principles calculations on the lattice at non-zero chemical potential (e.g., results of fluctuations of conserved charges such as baryon number, electric charge, and strangeness [117]). Also, it is interesting to study isentropic trajectories due to their importance for studying the thermodynamics of matter created in relativistic heavy-ion collisions.

The equations of state and other quantities of interest like the particle density (ρ_i), energy density (ϵ), and entropy density (S), can be derived from the thermodynamical potential $\Omega(T, \mu)$ (Equation (16)), using the following relations [118]:

$$p = -\Omega, \quad (32)$$

$$\rho_i = - \left(\frac{\partial \Omega}{\partial \mu_i} \right)_T, \quad (33)$$

$$S = - \left(\frac{\partial \Omega}{\partial T} \right)_\mu, \quad (34)$$

$$\epsilon = -P + TS + \sum_i \mu_i \rho_i. \quad (35)$$

The pressure and the energy density are defined in such way that their values are zero in the vacuum state [21].

2.5. Model Parameters and Regularization Procedure

Concerning the numerical calculations, the model is fixed by the coupling constants g_S , and g_D in the Lagrangian (1), the cutoff parameter Λ which regularizes momentum space integrals I_1^i (Equation (A2)) and I_2^{ij} (Equation (A3)), and the current quark masses m_i ($i = l, s$; with $m_u = m_d = m_l$). We employ the parameters of [45]. The (2 + 1)-flavors version of the NJL (PNJL) model has five parameters. These parameters are fixed in order to fit the observables $M_\pi = 135.0$ MeV, $f_\pi = 92.4$ MeV, $M_K = 497.7$ MeV, and $M_{\eta'}$ = 957.8 MeV, while $m_l = 5.5$ MeV. The parameters and the numerical results are given in Table 1.

Table 1. Physical quantities in the vacuum state and the parameter set used in this work. The asterisk signalize the results of the model for such physical quantities.

Physical Quantities	Parameter Set and Constituent Quark Masses
$f_\pi = 92.4$ MeV	$m_u = m_d = 5.5$ MeV
$M_\pi = 135.0$ MeV	$m_s = 140.7$ MeV
$M_K = 497.7$ MeV	$\Lambda = 602.3$ MeV
$M_{\eta'} = 957.8$ MeV	$g_S \Lambda^2 = 3.67$
$M_\eta = 514.8$ MeV *	$g_D \Lambda^5 = -12.36$
$f_K = 93.1$ MeV *	$M_u = M_d = 367.7$ MeV *
$M_\sigma = 728.9$ MeV *	$M_s = 549.5$ MeV *
$M_{a_0} = 880.2$ MeV *	
$M_\kappa = 1050.5$ MeV *	
$M_{f_0} = 1198.3$ MeV *	
$\theta_p = -5.8^\circ$ *; $\theta_S = 16^\circ$ *	

An important aspect of both, NJL and PNJL models, is the lack of renormalizability which comes from the point-like nature of the quark-quark interaction. As a consequence, a procedure for regularizing divergent quantities in both models is required. Therefore, the regularization scheme determines the model. As pointed out in [19], it is needed to look to physical and not just to the mathematical content. Therefore, the regularization process must be carried out in such a way that physically expected properties of the model and symmetry considerations are maintained [19].

Several regularization procedures are available: three dimensional cut-off [19], four dimensional cut-off [9,19,119] Pauli-Villars regularization [120–122], regularization in proper time [121,123]. For a detailed analysis of the regularization procedures and more references to the corresponding literature see [19,124,125].

In this work, we will use a three dimensional cut-off, Λ , in all integrals and not just the divergent ones. The effect of the inclusion of the Polyakov loop and the regularization procedure in the medium was studied in [93]. A regularization that includes high momentum quark states ($\Lambda \rightarrow \infty$ in finite integrals), is necessary to get the required increase of extensive thermodynamic quantities, allowing the convergence to the Stefan-Boltzmann (SB) limit of QCD. However, this leads to unphysical behavior of the quark condensates at very high temperatures (the quark condensates change sign because the constituent quark masses go below the respective current value) [126,127]. In Reference [128] a regularization procedure was proposed that prevents the unphysical behavior of the quark condensates ensuring, at the same time, that the pressure reaches the SB limit at high temperatures. On the other hand, in [129] it was shown that the inclusion of a temperature and chemical potential dependent term (which arises as a constant of integration when integrate the gap equations to obtain the thermodynamic potential) leads to the correct asymptotics for all observables considered.

The parameter T_0 is the temperature for the deconfinement phase transition in pure gauge. According to lattice findings, it is usually fixed to 270 MeV [130,131]. With this value of T_0 , an almost exact coincidence between the chiral crossover and the deconfinement transition at zero chemical potential is obtained, as seen in lattice calculations. However, different criteria for fixing T_0 are found in the literature as in [132] where an explicit N_f dependence of T_0 is given considering renormalization

group arguments. Since the results for the Polyakov loop coming from lattice calculations with $(2 + 1)$ flavors and with fairly realistic quark masses are identical to the $SU_f(2)$ case [133], it was chosen to maintain the same parameters that were used in $SU_f(2)$ PNJL [110] for the effective potential $\mathcal{U}(\Phi, \bar{\Phi}; T)$.

In the present work, we rescale T_0 to 195 MeV in order to get an agreement between the deconfinement pseudocritical temperature obtained in the model, with the results obtained on the lattice: 170 MeV [134]. This modification of T_0 (which is the only free parameter of the Polyakov loop since the effective potential is fixed) has a rescaling effect without drastically changing the physics of the model. With this choice of parameters, Φ and $\bar{\Phi}$ are always lower than 1.

To conclude this section, some comments regarding the the number of parameters and the nature of the Polyakov field are needed. It is important to mention that NJL parameters and the Polyakov potential are not on the same footing. In fact, while the NJL parameters can be directly related with physical quantities, the role of the Polyakov loop potential is to insure the recovering of pure gauge lattice expectations. This means that the potential for the Polyakov loop can be seen as an unique but functional parameter. The pure gauge critical temperature, T_0 , is the only true parameter and fixes the temperature scale of the system. However, in the Landau-Ginzburg framework, the characteristic temperature for a phase transition is not expected to be a prediction. Therefore, this parameter is changed in order to fix the correct energy scale and obtain the result for the deconfinement pseudocritical temperature, coming from lattice QCD calculations.

Finally it is important to point out that the Polyakov loop effective field is not a dynamical degree of freedom. This is due to the the absence of dynamical term in the Polyakov loop potential at the Lagrangian level: it is a background gauge field in which quarks propagate.

3. The Phase Diagram in the PNJL Model

We will start our analysis of the PNJL model by the respective phase diagram. We briefly discuss the chiral and deconfinement transitions as well as the Mott dissociation of the pion and sigma mesons at finite temperature and/or baryonic chemical potential. Isentropic trajectories will also be drawn and discussed.

3.1. Characteristic Temperatures at Zero Density

At zero temperature and density (baryonic chemical potential μ_B), the chiral symmetry of QCD is broken, both explicitly and spontaneously. It is then expected that chiral symmetry gets restored at high temperatures and an eventual phase transition will occur separating the regions of low and high temperatures.

We start the discussion of the results by identifying the characteristic temperatures, at $\mu_B = 0$, that splits the different thermodynamic phases in the PNJL model [27]. On the one hand, the pseudocritical temperature associated to the “deconfinement” transition is T_c^Φ . This temperature corresponds to the crossover location of Φ , defined by its inflexion point of, i.e., $\partial^2\Phi/\partial T^2 = 0$. The terminology “deconfinement” is used here to designate the transition between $\Phi \simeq 0$ and $\Phi \simeq 1$ (see Reference [27] for a detailed discussion of this subject). On the other hand, the chiral transition characteristic temperature, T_c^χ , is given by the inflexion point (chiral crossover) of the light chiral condensate $\langle \bar{q}_i q_i \rangle$ ($i = u, d$), i.e., $\partial^2 \langle \bar{q}_i q_i \rangle / \partial T^2 = 0$. However, since the presence of nonzero current quark mass terms break the chiral symmetry, the restoration of chiral symmetry is realized through parity doubling rather than by massless quarks. The temperature of *effective* restoration of chiral symmetry (in the light sector), T_{eff}^χ , is provided by the degeneracy of the respective chiral partners $[\pi, \sigma]$ and $[\eta, a_0]$ or, in other words, by the merging of their spectral functions [27,51]. T_{eff}^χ is then defined as the temperature where $M_\sigma - M_\pi < 1\%$ ($M_\sigma^{vac} - M_\pi^{vac}$) MeV. Indeed, one key point of this work is the effective restoration of symmetries through the mesonic properties perspective.

In Figure 1, the strange and nonstrange quarks condensates are plotted (left panel), as well as the respective quark masses (right panel), and the Polyakov loop as functions of the temperature.

In the left panel, we also plot the derivatives of the light quarks (black) and of the Polyakov loop (blue) in order to the temperature (thin lines). The respective peaks also indicate the pseudocritical temperatures for the partial restoration of chiral symmetry and the deconfinement. For temperatures near T_c^χ , the light quark masses drop in a continuous way to the respective current quark mass value. This indicates the smooth crossover from the chirally broken to a partially chirally symmetric phase, once the value of the quarks masses are still far from the value of the corresponding current masses (partial restoration of chiral symmetry). The strange quark mass shows a similar behavior to that of the nonstrange quarks, with a substantial decrease above T_c^χ ; however, its mass is still far away from the strange current quark mass. As in the NJL model, regarding the strange sector [47] and since $m_u = m_d < m_s$, the (sub)group $SU(2) \otimes SU(2)$ is a better symmetry of the Lagrangian (Equation (1)). This will have consequences in the behavior of the meson masses.

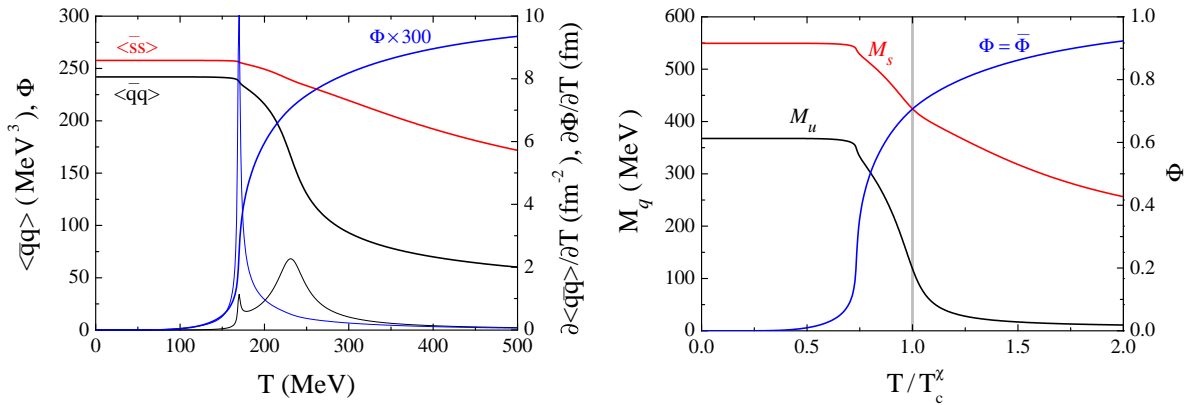


Figure 1. Quark condensates and respective derivatives (left panel) and quark masses (right panel) in the PNJL model as functions of the temperature; the Polyakov loop field, Φ , is also shown, together with its derivative given by the thin blue line in the left panel.

In Table 2, we report the characteristic temperatures in the PNJL model: the pseudocritical temperatures for the chiral transition (T_c^χ) and deconfinement (T_c^Φ); the effective chiral symmetry restoration temperature (T_{eff}^χ); and the Mott temperatures for pion (T_π^{Mott}), for eta (T_η^{Mott}), for kaon (T_{kaon}^{Mott}) and for the sigma (T_σ^{Mott}) mesons. We remind that the Mott transition is related with the composite nature of the mesons: at the Mott temperature it becomes energetically favorable for a meson to decay into a $\bar{q}q$ pair.

Table 2. Characteristic and Mott temperatures in the PNJL model at μ_B with $T_0 = 195$ MeV.

T_c^χ [MeV]	T_c^Φ [MeV]	T_{eff}^χ [MeV]	T_π^{Mott} [MeV]	T_η^{Mott} [MeV]	T_K^{Mott} [MeV]	T_σ^{Mott} [MeV]
231	170	280	239	211	243	197

The difference between T_c^Φ and T_c^χ is due to the choice of T_0 and the regularization procedure, as it was pointed out in Reference [27]. In these work a three-dimensional momentum cutoff to both the zero and the finite temperature/densities contributions is applied. Different type of regularizations can lower T_c^χ [126]. In Reference [93] the meson properties were calculated without rescaling the parameter T_0 to a smaller value. By adopting a higher value of T_0 , a smaller difference between the pseudocritical temperatures of the two transitions was obtained. However, since our goal is the general properties of mesons, the absolute value of the pseudocritical temperatures is not the most significant point: in fact, these properties are independent of the precise value of T_c^χ and different values of T_0 do not change the conclusions.

3.2. Finite Temperature and Chemical Potential

Now, let's extend the analysis to the scenario with $\mu_B \neq 0$, i.e., the phase diagram. The PNJL model can mimic a region in the interior of a neutron star (where the PNJL model is reduced to the NJL model) or a dense fireball created in a HIC. Bearing in mind that in a relativistic HIC, the fireball evolves rapidly (it takes about 10^{-22} s for hadronization), only processes mediated by the strong interaction will attain thermal equilibration rather than the full electroweak equilibrium. In this work, we impose the condition $\mu_u = \mu_d = \mu_s = \mu_q$ (equal quark chemical potentials) with $\mu_B = 3\mu_q$. This corresponds to zero charge (or isospin), $\mu_Q = 0$, and zero strangeness chemical potential, $\mu_S = 0$. This choice also allows for isospin symmetry, $M_u = M_d$. The net strange quark density, ρ_S , will be different from zero but only at very high values of T and/or μ_B .

From both panels of Figure 2 one can see that, instead of what happens at finite temperature, at $T = 0$ and finite baryonic chemical potential a first-order phase transition takes place with the critical chemical potential being $\mu_B^{crit} = 1083$ MeV (or $\mu_q^{crit} = 361$ MeV). As the temperature increases this first-order transition (blue full line) persists up to the chiral CEP (black dot). Along this line, the thermodynamic potential has two degenerate minima which are separated by a finite potential barrier. The two minima correspond to the phases of broken and restored chiral symmetry, respectively. As the temperature increases the height of the barrier decreases and disappears at the CEP, which is located at $T^{CEP} = 126.3$ MeV and $\mu_B^{CEP} = 915.4$ MeV ($\rho_B^{CEP} = 1.75\rho_0$). At the CEP the chiral transition becomes a second-order phase transition.

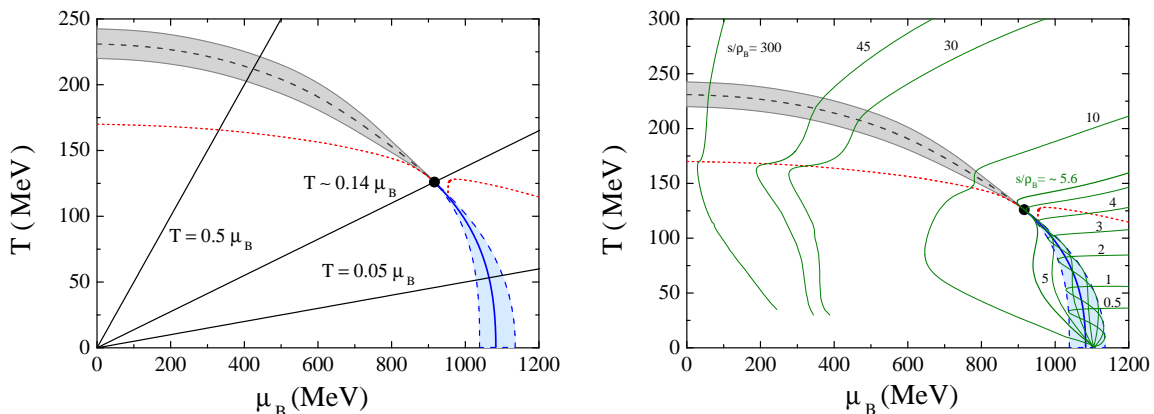


Figure 2. (Left panel) Deconfinement transition (red dots) and chiral transition with first-order (full blue line), CEP (black dot) and crossover regions (dashed black line) and spinodal lines (dashed blue line). (Right panel) Deconfinement and chiral transitions alongside isentropic lines (full green lines).

The blue dashed lines in Figure 2 are the borders of the coexistence area (light blue region). The domain between these lines has metastable states, characterized by large fluctuations. Although they are also solutions of the gap equations, their thermodynamic potential is higher than for the stable solutions. The left dashed curve is the beginning of the metastable solutions of restored symmetry in the phase of broken symmetry, while the right dashed curve depicts the end of the metastable solutions of broken symmetry in the restored symmetric phase. Above the CEP the thermodynamic potential has only one minimum, meaning that the transition is washed out and only a smooth crossover occurs (gray dashed line).

The crossover is a fast decrease of the chiral order-like parameter (the quark condensate) and its range is defined by the interval between the two peaks around the zero of $\partial^2 \langle \bar{q}_i q_i \rangle / \partial T^2$. In Figure 2 this region is presented in gray. It can be seen that, as μ_B increases, the area where the crossover takes place is getting narrower and narrower until it reaches the CEP.

3.3. Nernst Principle and Isentropic Trajectories

It is accepted that the expansion of the QGP in HIC is a hydrodynamic expansion of an ideal fluid and it will nearly follow trajectories of constant entropy. Due to the baryon number conservation, the isentropic trajectories are lines of constant entropy per baryon, i.e., s/ρ_B , in the (T, μ_B) -plane and contain relevant information on the adiabatic evolution of the system. The values of s/ρ_B for AGS, SPS, and RHIC, are 30, 45, and 300, respectively [135].

The numerical results for the isentropic trajectories in the (T, μ_B) -plane are given in the right panel Figure 2. A complete study of the behavior of isentropics trajectories in the PNJL model under the influence of a repulsive vector interaction and by the presence of an external magnetic field was performed in [136]. It is important to start the discussion by analyzing the behavior of the isentropic trajectories when $T \rightarrow 0$. In this limit, $s \rightarrow 0$ according to the third law of thermodynamics and, once also $\rho_B \rightarrow 0$, it is insured the condition $s/\rho_B = \text{const.}$. In fact, all isentropic trajectories end at the same point ($T = 0$ and $\mu_q = \mu_B/3 = 367.7$ MeV) of the horizontal axes. Since $\mu_q = M_q^{\text{vac}} > \mu_q^{\text{crit}}$, the combination ($T = 0, \mu_q = 367.7$ MeV) corresponds to the vacuum. With the chosen set of parameters, the point where the first-order transition occurs satisfies the condition $\mu_q^{\text{crit}} < M_q^{\text{vac}}$ for $T = 0$ [21]. It also allows the existence of a strong first-order phase transition from the vacuum solution, $M_q = M_q^{\text{vac}}$, into the partially chiral restored phase with M_q smaller than M_q^{vac} . At the transition point, the total baryonic density jumps from zero to $2.5\rho_0$, equally carried by u and d -quarks (the density of strange quarks, ρ_s , is still zero, and the system only has $\rho_s \neq 0$ when $\mu_q > M_s$).

Close to the first-order region, for $T \neq 0$, the isentropic trajectories ($s/\rho_B = 1, \dots, 5$) show the following behavior: they come from the region of partially restored chiral symmetry reaching the unstable region (spinodal region), delimited by the spinodal lines, going then along with it as T decreases until they reach $T = 0$. By looking to the trajectory $s/\rho_B = 0.5$, it can be seen that the isentropic trajectory crosses the spinodal line at ($T \approx 36$ MeV, $\mu_B \approx 1122$ MeV) and intersects the first-order line twice, at ($T \approx 35$ MeV, $\mu_B \approx 1075$ MeV) and ($T \approx 25$ MeV, $\mu_q \approx 1080$ MeV), as the temperature decreases in a “zigzag”-shaped trajectory delimited by the spinodal lines. By analyzing the isentropic trajectory with $s/\rho_B = 5$, it is interesting to notice that it starts by having an identical behavior to the isentropic trajectory $s/\rho_B = 0.5$, but it then leaves the spinodal region. Nonetheless, as the temperature diminishes, the isentropic trajectory reaches once again the spinodal region, now from lower values of μ_B . After that, it also goes to the horizontal axes ($T = 0$). The isentropic trajectory $s/\rho_B = 5.6$ nearly goes through the CEP and we will calculate the meson masses along this path.

Concerning the behavior of the isentropic trajectories in the chiral crossover region, ($s/\rho_B > 5.6$) it is qualitatively similar to the one obtained in lattice calculations [137,138] or in some models [139–141]: they directly go through the crossover region, displaying a smooth behavior. However, they suffer a pronounced bend when they cross the deconfinement transition (red dashed curve) reaching the spinodal region from lower values of μ_B . In conclusion, all the trajectories directly arrive in the same point of the horizontal axes at $T = 0$.

A final remark; while the critical behavior at the CEP is universal, characteristic shape of the isentropic trajectories near the CEP can change from model to model, even if they belong to the same universality class [142].

4. Scalar and Pseudoscalar Mesons in the PNJL Model

In this section, we will study the behavior of scalar and pseudoscalar mesons in the PNJL model for different physical scenarios. We will look for signs of the effective restoration of chiral symmetry and how the chiral transition and the deconfinement affect their behavior. The criterion to identify an effective restoration of the chiral symmetry will be to seek for the degeneracy of the respective chiral partners. Indeed, we will compare the properties (e.g., the masses) of the pseudoscalar meson nonet (π, K, η , and η') with those which can be considered as chiral partners, i.e., the scalar mesons (σ, κ, a_0 , and f_0).

4.1. Mesons Properties at Finite Temperature

4.1.1. Mesonic Masses and Mixing Angles

We start with the analysis of the mesons and mixing angles general behavior. The plot of the meson masses, mixing angles and coupling constants will be done as functions of the reduced temperature T/T_c^χ . This will allow a better understanding of their behavior around the chiral pseudocritical temperature. The masses of the pseudoscalar mesons π , K , η , and η' (solid lines) and of the respective scalar chiral partners σ , κ , a_0 , and f_0 (dashed lines) as functions of the reduced temperature are given in the left panel of Figure 3.

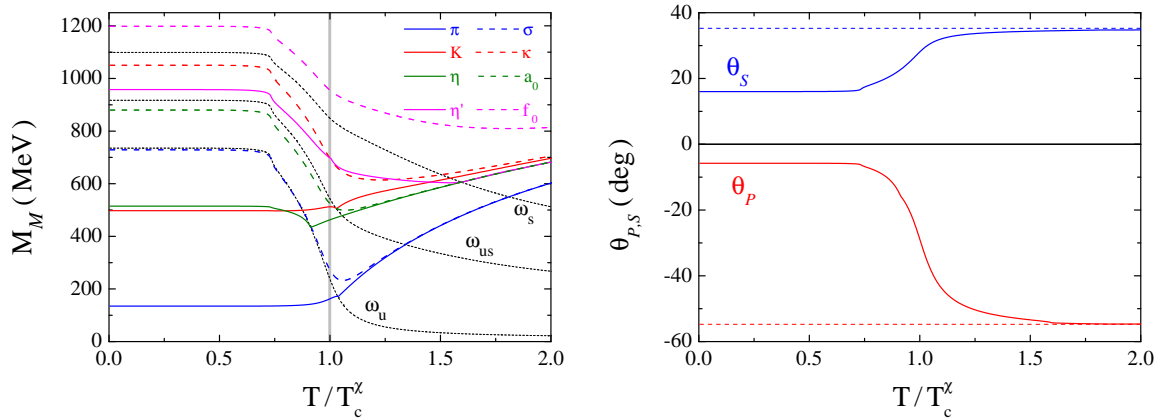


Figure 3. (Left panel) Masses of the pseudoscalar (full lines) and scalar mesons (dashed lines) as function of the reduced temperature. (Right panel) Pseudoscalar and scalar mixing angles as a function of the reduced temperature.

Concerning the pseudoscalar mesons, they are bound states at low temperature (except the η' meson that is always above the continuum $\omega_u = 2M_u$), but they become unbound at the respective Mott temperatures (see Table 2). The Mott temperature is the temperature where the transition from a bound state to a resonance takes place and, as already pointed out, it comes from the fact that mesons are not elementary objects but composed states of $\bar{q}q$ excitations. Above the Mott temperature, the imaginary parts of the integrals I_2^{ij} (see Equation (A3)) must be taken into account and the finite width approximation is used [45]. The lower limits of the continua belonging to each meson are also shown (black dotted lines). Indeed, the continuum starts when the π , and the η masses cross the quark threshold $\omega_u = 2M_u$ and the K crosses $\omega_{us} = M_u + M_s$. For the π and K mesons this entry into the continuum occurs at approximately the same temperature ($T_\pi^{Mott} = 239$ MeV, $T_K^{Mott} = 242$ MeV). The η' meson is always an unbound state and its mass already begins to be larger than $\omega_u = 2M_u$.

Concerning the scalar mesons, the σ -meson is the only scalar meson that can be considered as a true (slightly) bound state for relatively small temperatures. At the corresponding Mott temperature, $T_\sigma^{Mott} = 197$ MeV, it turns into a resonance. The other scalar mesons are always resonant states. For the π , η and σ there is a second entry into the continuum when the mass of these mesons intersect $\omega_s = 2M_s$.

As shown in Ref. [127], at T_{eff}^χ the behavior of some observables signalize the so-called effective restoration of chiral: the masses of the meson chiral partners become degenerate as it can be seen in Figure 3 (left panel). In this case, for temperatures above 280 MeV the π starts to be degenerate with the σ meson. It also can be seen that the partners $[\pi, \sigma]$ (blue curves) and $[\eta, a_0]$ (green curves) become degenerate at almost the same temperature. In both cases, this behavior is a clear indication of the effective restoration of chiral symmetry in the nonstrange sector. Differently, the masses of η' and f_0 mesons do not show a tendency to converge in the range of temperatures considered. This pattern can be interpreted as a sign that chiral symmetry does not show a trend to get restored in the strange sector, a consequence of the slow decrease of M_s in Figure 1 (right panel).

Finally, our attention will be focused in the K and κ mesons (red curves in the left panel of Figure 3). The κ is always unbounded and it exhibits a tendency to get degenerate in mass with the K meson for increasing temperatures.

Summarizing the above, the SU(2) chiral partners $[\pi, \sigma]$ and $[\eta, a_0]$ become degenerate for temperatures higher than $T > 280$ MeV (the masses of the σ and η mesons become less strange, and converge, respectively, with the non strange ones, π and a_0); the $[\eta', f_0]$ do not indicate a tendency to converge in the range of temperatures studied; the convergence of the partners K and κ that have a $\bar{u}s$ structure, occurs at higher values of the temperature, and is presumably slowed down by the small decrease of the strange quark mass, M_s . The degree of restoration of chiral symmetry in the different sectors essentially drives the mesonic behavior.

It is important to refer that, as pointed out in [51], the behavior of the mesonic masses in the PNJL model is qualitatively similar to the corresponding one in the NJL model [47,116,143].

Concerning the pseudoscalar mixing angle, θ_P , a first evidence emerges from the right panel of Figure 3: as the temperature increases, it goes to its ideal value $\theta_P = -54.736^\circ$ asymptotically. As a result, a remarkable change in the quark content of the mesons η and η' occurs, although a small percentage of mixing always remains: the η eventually becomes almost nonstrange, while the η' becomes almost a purely strange meson [47,143]. The scalar mixing angle θ_S shows an identical tendency: the ideal mixing angle goes asymptotically to $\theta_S = 35.264^\circ$. Therefore, there is a decrease of the strange component of the σ -meson, that never disappears, and f_0 becomes almost purely strange.

The mixing angles are very sensitive to temperature (and also the medium) effects, particularly due to its influence on the mass of strange quark. This might be an explanation to the fact that some aspects of θ_S and θ_P behavior are not the same in different models [144,145]. It should be noticed that the mixing angles depend on the mesons masses, namely, θ_S on the mass of the σ -meson and θ_P on the mass of the η -meson.

The evolution of the strangeness content of both mesons, η and η' determines which meson will become nonstrange, and consequently will behave as the chiral axial partner of the π . The behavior of θ_P at finite temperature leads to the identification of the η as the chiral axial partner of the π , but the opposite is found in References [144,146] where a crossing of the mixing angles can be seen. A certain degree of crossing of the pseudoscalar mixing angle and exchange of identities of η , η' was also seen in Reference [147], and an alike effect for the scalar angle was presented in Ref. [144]. Indeed, because of the mixing angles behavior, f_0 and η' become essentially strange for increasing temperatures. Besides, as it was shown in Reference [126], even when the spontaneously broken chiral symmetry gets restored in all sectors (and unlike what is found for the nonstrange chiral partners) a considerable difference between the masses of these mesons is still present, a fact due to the high value of the current strange quark mass used in this work ($m_s = 140.7$ MeV). Indeed, at high temperatures the relation $m_{f_0}^2 \simeq m_{\eta'}^2 + 4m_s^2$ is approximately valid, thus explaining the observed behavior.

4.1.2. Pion and Kaon Coupling Constants

The left(right) panel of Figure 4 shows the values of the π and K coupling(decay) constants. At the Mott temperature, a striking behavior for each meson can be seen: the coupling strengths approach zero for $T \rightarrow T_{\pi(K)}^{Mott}$ [45]. This behavior occurs because the polarization displays a kink singularity, which can also be seen in the meson masses.

It is interesting to note that the Mott temperature for each meson is above T_c^χ , indicating a slightly survival of these mesons as bound states in the restored phase. This is a feature of the PNJL model, which is a quantitative step toward confinement regarding the NJL model. This is due to the Φ factor that suppresses the 1- and 2- quarks Boltzmann factor at low temperatures. Indeed, the fast restoration of the \mathbb{Z}_3 symmetry (Φ goes to one with increasing temperatures) produces a quark thermal bath with all (1-, 2- and 3-) quark contributions in a short range of temperatures, which might help to explain the fastening of the transition [51].

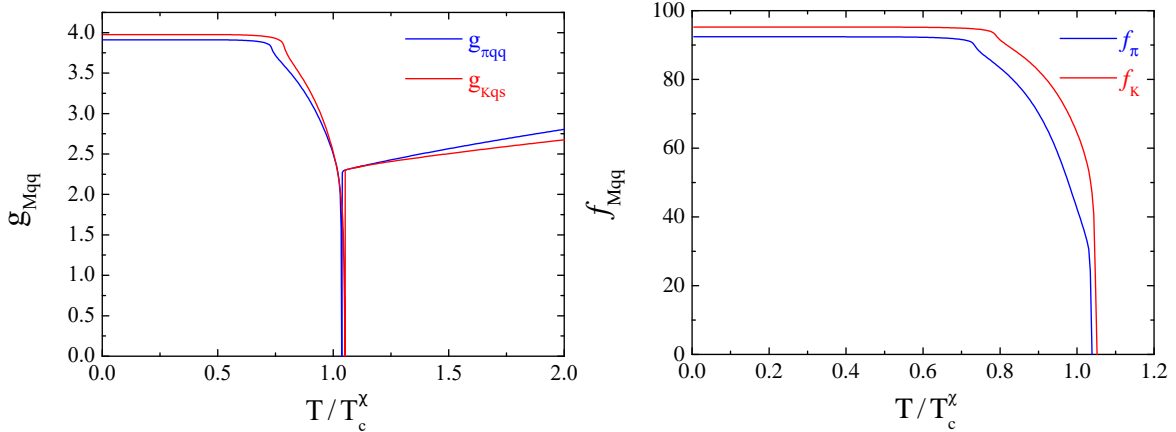


Figure 4. Coupling constants (left panel) and decay constants (right panel) as a function of the reduced temperature.

4.2. Mesons at Zero Temperature

Next, we will study the meson behavior at finite values of μ_B . We emphasize that, as previously stated, the employed PNJL model at $T = 0$ is identical to the usual NJL model.

We consider symmetric quark matter as in Section 3.2. The first aspect that arises is that, similarly to the previous finite temperature scenario, chiral symmetry is effectively restored only in the light sector. This is due to some specific details of the behavior of the strange quark mass with the density. Figure 5 shows the quark masses as function of μ_B around the first-order transition, left panel, and as a function of ρ_B/ρ_0 , right panel (the light-blue area corresponds to the region of the phase transition). As it can be seen, in the present case there are no strange quarks in the medium at low densities. The mass of the strange quark smoothly decreases, due to the effect of the 't Hooft interaction, and it becomes smaller than the chemical potential for strange quarks (at $\rho_B \simeq 5.45\rho_0$ and $\mu_B \simeq 1388$ MeV) and strange quarks appear in the system. Then, a pronounced decrease of the strange quark mass is observed.

With respect to the meson spectra and the mixing angles, we will discuss new aspects that arise, mainly in the high baryonic chemical potential/density region.

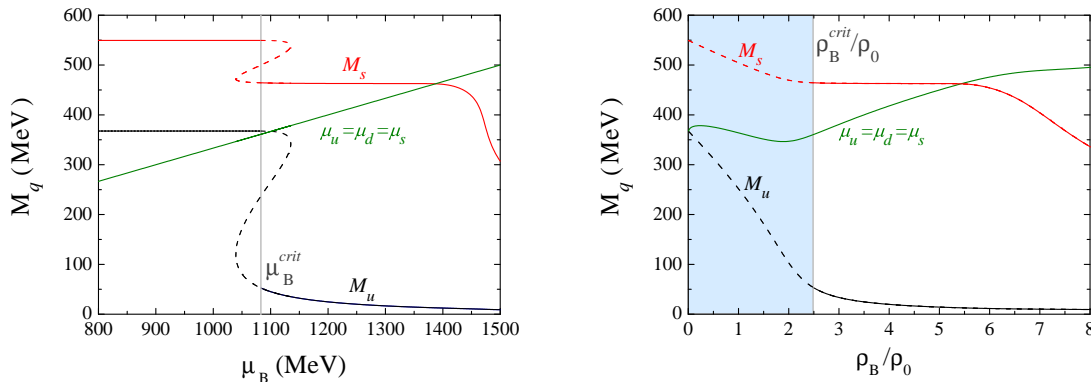


Figure 5. Quark masses at $T = 0$ as a function of the baryonic chemical potential (left panel) and reduced baryonic density (right panel). The dashed lines represent the quark masses in the first-order region. μ_B^{crit} is the baryonic critical chemical potential of the first-order phase transition, and ρ_B^{crit}/ρ_0 the respective critical reduced density ($\rho_0 = 0.16 \text{ fm}^{-3}$).

In Figure 6, the meson masses are plotted as functions of the baryonic chemical potential (panel (a)) and of the density (panel (b)). The chiral partners $[\pi, \sigma]$ (blue curves) are always bound states. Before continuing the discussion, some words about the continuum ω' at zero temperature are

needed. From the dispersion relations for the pion and kaons, at $T = 0$, two kinds of discrete bound states are allowed (looking to the limits of the regions of poles in the integrals I_2^{ij} , Equation (A3)): particle-antiparticle modes of the Dirac sea, that are already present in the vacuum and are related with the spontaneous breaking of chiral symmetry; and, when the breaking of the flavor symmetry is considered, particle-hole excitations of the Fermi sea, that only manifest themselves in the medium (for a detailed description, see [42]). On the other hand, the Fermi and Dirac sea continua are defined by the unperturbed solution. In the isospin limit, the Dirac continuum starts at $\omega' = \omega'_{u(d)} = 2\mu_{u(d)}$ and at $\omega'_s = 2\mu_s$ (at finite temperature, we have $\omega_{u(d)} = 2M_{u(d)}$, and $\omega_s = 2M_s$).

Returning to meson masses, for all range of densities (chemical potentials), the pion is a light quark system contrary to the σ meson which has a strange component at $\rho_B = 0$ but never becomes a purely non-strange state because θ_S never reaches the ideal mixing angle 35.264° (Figure 6, panels (c) and (d)). As ρ_B (μ_B) increases these mesons become degenerate ($\rho_B^{eff} \gtrsim 2.9\rho_0$, $\mu_B^{eff} \gtrsim 1126$ MeV, effective restoration of chiral symmetry in the light sector, see blue curves of panels (a) and (b)).

At the approximate same density, and μ_B , the chiral partners $[\eta, a_0]$ (green curves in panels (a) and (b) of Figure 6) also become degenerate. On one hand, the η -meson is permanently a bound state; on the other hand, a_0 starts to be a resonance, because its mass is above the $\bar{q}q$ continuum, and converts into a bound state for $\rho_B \gtrsim 0.6\rho_0$, and $\mu_B \gtrsim 1121$ MeV.

However, as the baryonic chemical potential (panel (a)) or the density (panel (b)) increases, the a_0 mass splits from the η mass and goes to degenerate with the η' mass. To clarify this behavior we look to the behavior of the mixing angle θ_P in panels (d) and (e) of Figure 6: it is noticed that the angle θ_P , which starts at -5.8° , changes sign at $\mu_B \simeq 1167$ MeV ($\rho_B \simeq 3.2\rho_0$) becoming positive and increasing rapidly, which can be interpreted as a signal of a change of identity between both η and η' mesons. As it was seen in Figure 5, the strange quark mass decreases more rapidly when strange quarks appear in the system ($\mu_q > M_s$). A consequence of this behavior is the changing in the percentage of strange, $(q\bar{q})_s = s\bar{s}$, and non-strange, $(q\bar{q})_{ns} = \frac{1}{2}(u\bar{u} + d\bar{d})$, quark content in η and η' mesons: the η' has a bigger strangeness component than the η at low density, and the opposite takes place at high density [143]. Then, the η' mass will degenerate with the mass of the a_0 -meson that is permanently a non-strange state. As a final point, the f_0 -resonance is a strange state for all densities that denotes a tendency to be degenerated with other mesons only at very high values of μ_B (ρ_B).

A very interesting scenario happens for kaons and their chiral partners: K^\pm and κ^\pm (Figure 5, panels (e) and (f)). A first finding concerns to the separation between charge multiplets of kaons and the respective κ -mesons. Also the mass degeneracy of $[K^+, \kappa^+]$ and $[K^-, \kappa^-]$ occur at different values of density (chemical potential) which are higher then for $[\pi, \sigma]$. Indeed, taking the difference ($M_{K^\pm} - M_{\kappa^\pm}$), now at 5% of its vacuum value, for $[K^+, \kappa^+]$ the degeneracy of their masses takes place at $\mu_B = 1187$ MeV ($\rho_B = 3.38\rho_0$) while for $[K^-, \kappa^-]$ the degeneracy takes place at $\mu_B = 1419$ MeV ($\rho_B = 5.86\rho_0$).

Another particularity is the fact that the K^+ is always a bound state, never reaching the continuum, while the K^- is bounded only until it gets in the continuum of $s\bar{u}$ excitations of the Dirac sea at $\mu_B = 1083$ MeV ($\rho_B = 2.5\rho_0$) and becomes thereafter a $s\bar{u}$ resonance: $M_{K^-} > \omega_{us}^{(1)}$ (with $\omega_{us}^{(1)} = (M_s^2 + \lambda_u^2)^{1/2} + \mu_u$, being the chemical potential $\mu_u = (M_u^2 + \lambda_s^2)^{1/2}$, and the Fermi momentum of the i -quark $\lambda_i = (\pi^2\rho_i)^{1/3}$). However, when $\mu_B > 1419$ MeV ($\rho_B > 5.85\rho_0$) the K^- becomes once again a bound state (this behavior was already found in [116,148]). Still as far as the K^- is concerned, it was shown in [41,42,47,148] that there are low bound states with quantum numbers of K^- that appear below the inferior limit of the Fermi sea continuum of particle-hole excitations being the Fermi sea bounded by $\omega_{low} = (M_s^2 + \lambda_u^2)^{1/2} - \mu_u$ and $\omega_{up} = (M_s^2 + \lambda_s^2)^{1/2} - (M_u^2 + \lambda_s^2)^{1/2}$. However, we will not go further in this discussion.

Finally, with respect to the scalar mesons, κ^\pm , it is verified that both mesons start to be unbounded, with the continuum now defined as $\omega_{us}^{(2)} = \mu_s + (M_u^2 + \lambda_s^2)^{1/2}$ (at $T = \rho_B = 0$ $\omega_{us}^{(1)} = \omega_{us}^{(2)}$) but, as μ_B (ρ_B) increases, they will turn into bound states and become degenerated with the respective partners.

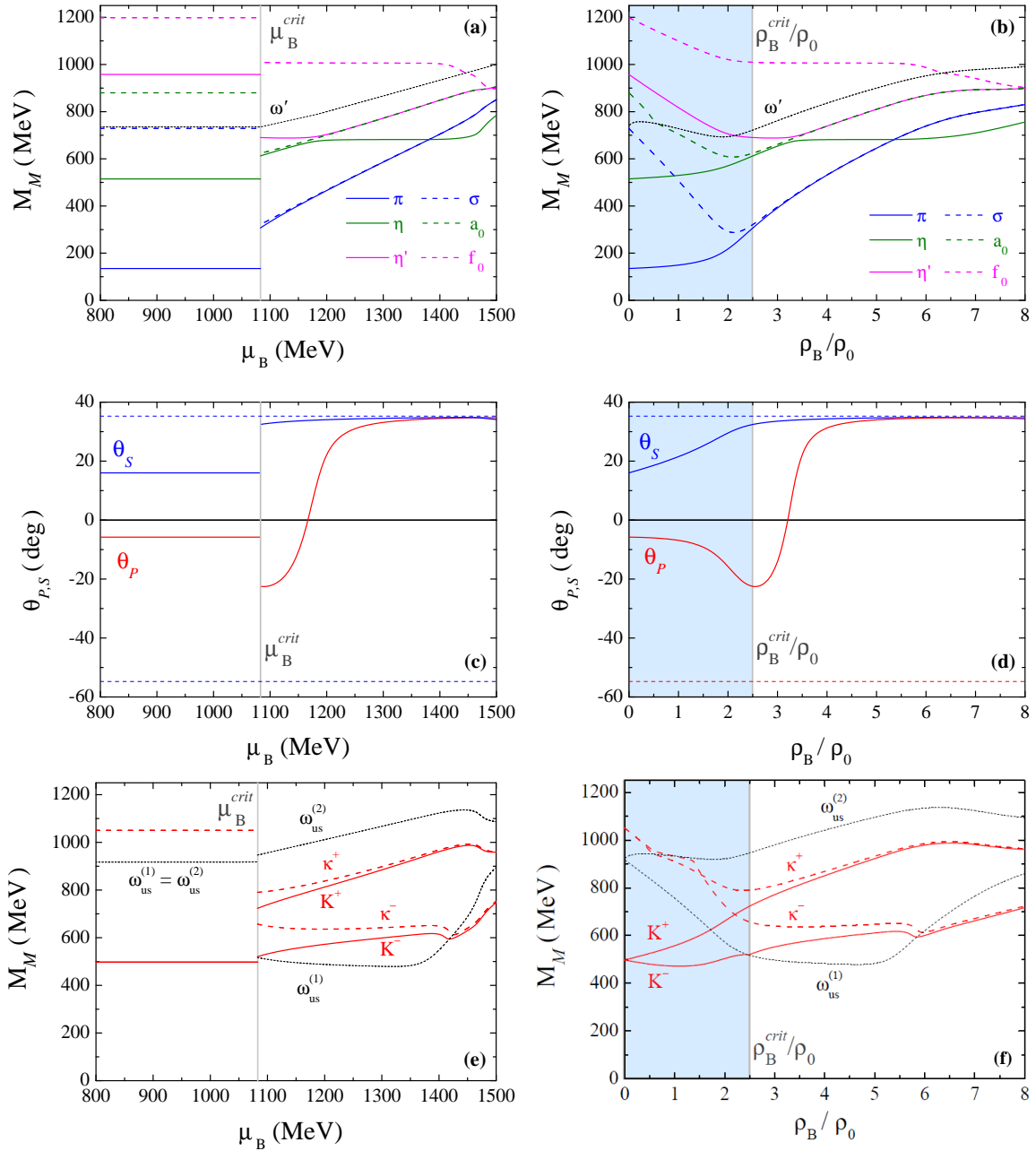


Figure 6. Masses of the neutral pseudoscalar and scalar mesons as a function of μ_B (panel (a)) and as a function of ρ_B/ρ_0 (panel (b)); the pseudoscalar and scalar mixing angles as a function of μ_B (panel (c)) and as a function of ρ_B/ρ_0 (panel (d)); masses of the charged pseudoscalar and scalar mesons as a function of μ_B (panel (e)) and as a function of ρ_B/ρ_0 (panel (f)). All results are at $T = 0$ (see text for details).

4.3. Mesons Properties in Different Regions of the Phase Diagram

4.3.1. Meson Masses in the Crossover Region

We continue the analysis of the behavior of mesons masses in symmetric matter, by following a path in the $(T - \mu_B)$ -plane passing through the crossover region. As indicated in Figure 2, we choose the path $T = 0.5\mu_B$. Chiral symmetry is, again, effectively restored only in the light quark sector.

In Figure 7 the meson masses are plotted as functions of temperature and baryonic chemical potential, in the left panels and right panels, respectively.

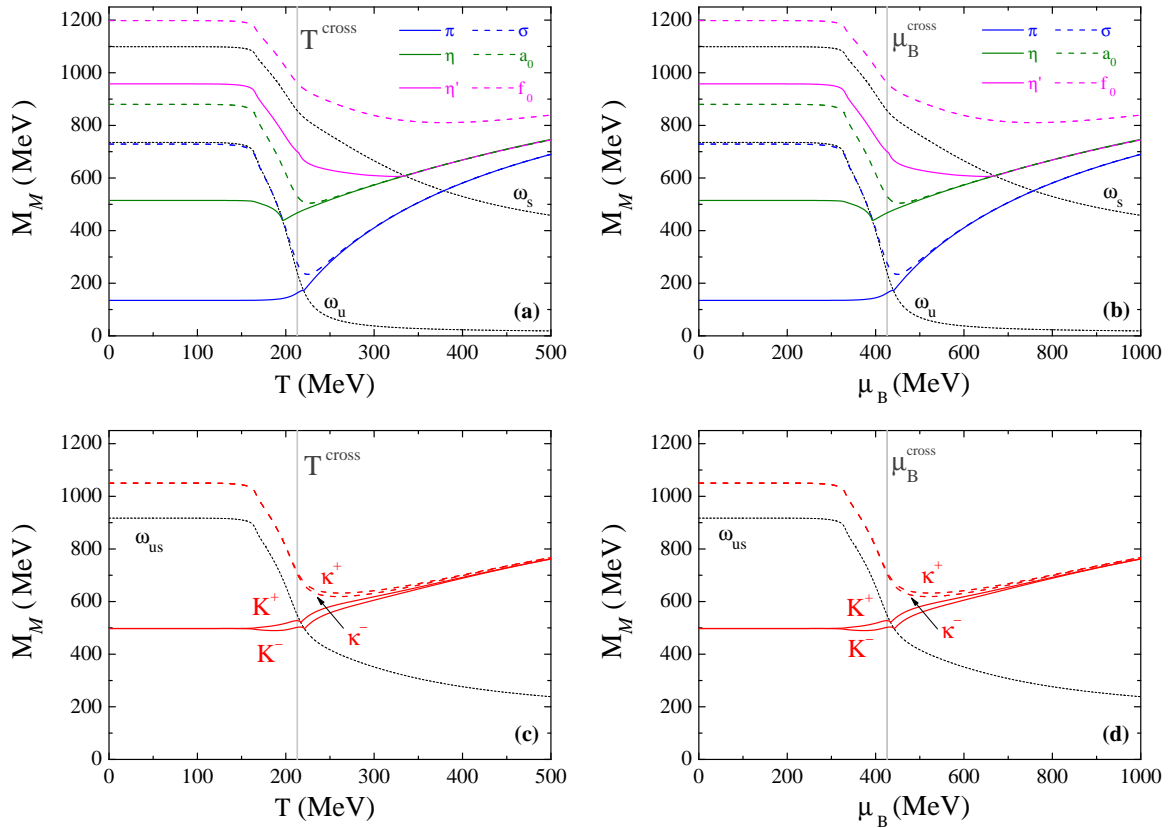


Figure 7. Masses of the pseudoscalar and scalar mesons as function of the temperature (panels (a,c)) and as function of μ_B (panels (b,d)) along the path $T = 0.5\mu_B$, the crossover region. $T^{\text{cross}} = 213$ MeV and $\mu_B^{\text{cross}} = 426$ MeV are, respectively, the temperature and the baryonic chemical potential for the crossover.

The chiral partners $[\pi, \sigma]$ and the η meson are bound states up to the respective Mott dissociation for a certain temperature and chemical potential (density) as can be seen in panels (a) and (b) Figure 7. The pion still survives as a bound state after the crossover transition in a small range of temperatures and chemical potentials.

Differently from the zero temperature case, and like the case at finite temperature and zero density, the a_0 meson is always a resonance since its mass always lies above the $\omega_u = 2M_u$ continuum (see Figure 7 panel (a) and (b)). As in the zero temperature case, the degeneracy between each set of chiral partners, $[\pi, \sigma]$ and $[\eta, a_0]$, happens at almost the same temperature and chemical potential.

The η' meson is always a resonance state and it will reach the $\omega_s = 2M_s$ continuum, a temperature and a chemical potential where it can decay also in a $\bar{s}s$ pair. Immediately, it degenerates with the η and a_0 mesons. Its chiral partner, f_0 , is always above the $\omega_s = 2M_s$ continuum.

Concerning the kaons and their chiral partners (Figure 7, panels (c) and (d)), the previously observed charge splitting at $T = 0$ MeV is also present (contrasting with the case $\mu_B = 0$ MeV where no splitting occurs). However, its effect is much less visible than in the zero temperature case and it happens, for the K^\pm , before the crossover while for κ^\pm it happens after the critical temperature and chemical potential. Both K^+ and K^- are bound states until they reach the $\omega_{us} = M_u + M_s$ continuum while their chiral partners, are always resonances. The continuum is reached slightly above the critical temperature and baryonic chemical potential of the crossover transition.

The degeneracy mechanism for these mesons in this path is different from previously studied zero temperature case. Since the charge splitting in this scenario is much less severe, we first

observe degeneracy between each charge multiplet K^\pm and κ^\pm , happening at approximately the same temperature and chemical potentials. Following this behavior the chiral partners $[K, \kappa]$ become degenerate at higher values of temperature and baryonic chemical potential.

At high enough temperatures and chemical potentials (outside the range of applicability of the model) it is expected that all mesons become degenerate.

4.3.2. Mesons through the CEP

In this subsection we explore the meson behavior along a path that goes through the CEP. This path can be parameterized by $T = 0.14 \mu_B$, as seen in Figure 2. The meson masses are plotted as functions of temperature and chemical potential, in the left panels and right panels of Figure 8 respectively.

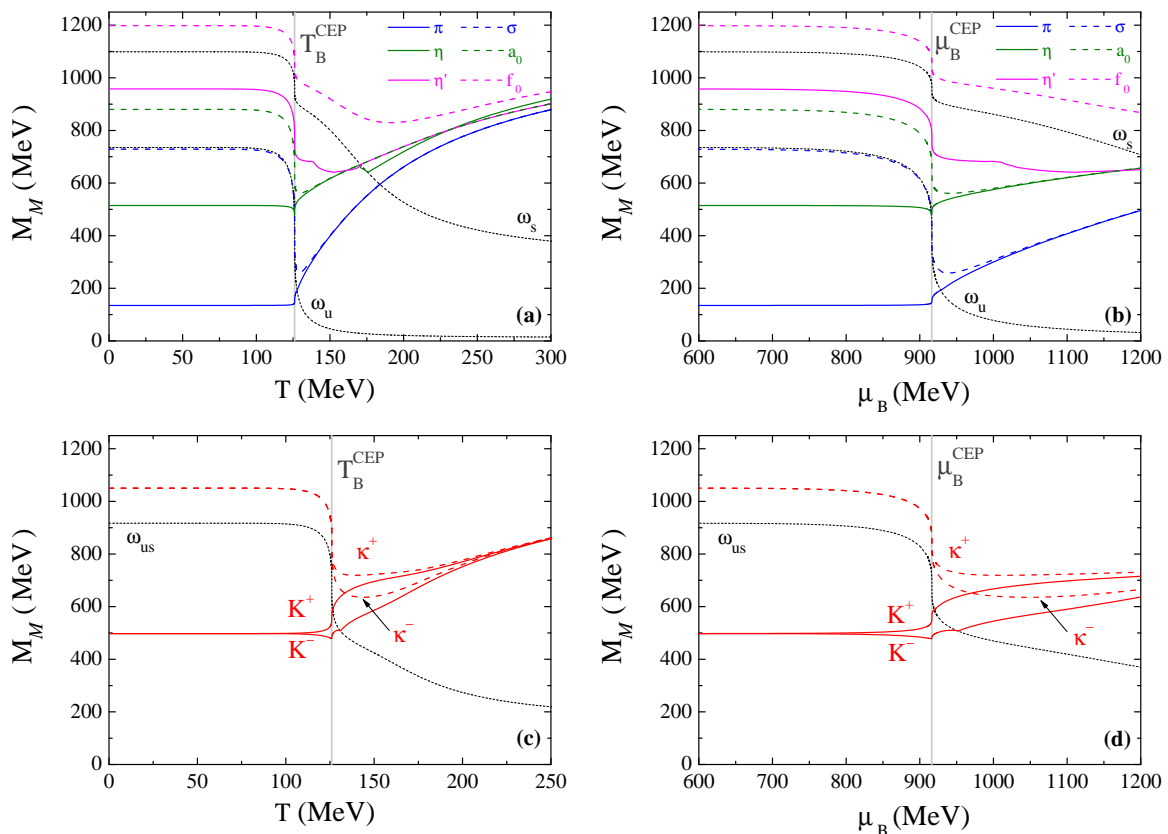


Figure 8. Masses of the pseudoscalar and scalar mesons as function of the temperature (panels (a,c)) and as function of μ_B (panels (b,d)) along the path that crosses the CEP.

We first discuss the behavior of the $[\pi, \sigma]$, $[\eta, a_0]$ and $[\eta', f_0]$ meson masses presented in panels (a) and (b) of Figure 8. The main and most important observation from Figure 8 is the drastic continuous decrease that almost meson masses (except the pion and K^+) displays in the temperature and chemical potential of the CEP. In fact, this feature may be used as a signal for the CEP. For example, processes such as $\sigma \rightarrow \pi\pi$ and $\sigma \rightarrow \gamma\gamma$ productions are important tools for the search of the CEP [149,150]. If the σ -meson has an abnormally small mass around the CEP, this means that peculiar experimental signatures are expected to be observed through its spectral changes: the dipion decay can be suppressed near the CEP due to the fast reduction of the σ -meson mass. Also the maximum in the K^+/π^+ ratio (“the horn” effect) [151], that was discussed as a possible signal of the onset of deconfinement, that also appears near CEP (being considered as a critical region signal for the CEP [152]), can be related with the increase of the K^+ mass seen in Figure 8 (panels (c) and (d)) relative to the decreasing K^- mass.

The σ and η mesons are bound states up to the CEP, where both mesons reach the ω_u continuum. The pion survives as a bound state after the CEP for a very limited range of temperatures and chemical

potentials, reaching the continuum after the CEP. After becoming resonances, the chiral partners $[\pi, \sigma]$ degenerate. The η' -meson mass is bigger than the ω_u continuum, meaning it is always unbound. The $[\eta, a_0]$ also become degenerate up to the ω_s continuum where the η (green curve) and η' (magenta curve) switch roles (this is particularly seen in panel (a) of Figure 8 with the mesons as functions of the temperature), as we will discuss in the following. The f_0 meson is a resonance and its mass is always above the ω_s continuum.

The η' mass reaches the ω_s continuum at $\sim 1.4T^{\text{CEP}}$ and $\sim 1.4\mu_B^{\text{CEP}}$. Then, the η and η' switch nature since the η' immediately become degenerate with the a_0 meson while the η meson separates from the a_0 mass and asymptotically degenerates with the f_0 meson mass.

As in the crossover scenario, there is charge splitting before and after the CEP for the K^\pm and κ^\pm , respectively (see panels (c) and (d) of Figure 8). The splitting for kaons become even more pronounced just at the CEP. The K^+ is a bound state up to the CEP where it reaches the ω_{us} continuum while the K^- is a bound state that survives the CEP, for a limited range of temperature and chemical potential. After becoming resonances, the both kaons will degenerate with the respective chiral partners of the same charge, κ^\pm , being these scalar mesons always resonances. The charge splitting between mesons disappears as temperature and chemical potential increases (faster for the temperature).

4.3.3. Mesons through the First-Order Transition

We now analyze a path that goes through the first-order phase transition, parameterized by $T = 0.05 \mu_B$ (see Figure 2). In the right and left panels of Figure 9, are displayed the mesons masses as functions of the temperature and chemical potential for this scenario.

The general behavior of the mesons in this case is very similar to the one encountered in the zero temperature case since, in both cases, there is a first-order phase transition. However, there are some specifications.

The π , σ and η mesons are bound states up to the phase transition. Immediately after this point they, discontinuously, become resonances. In fact, the discontinuity in the meson masses is a consequence of the nature of the first-order phase transition where the thermodynamical potential has two degenerate minima and there is a discontinuous jump from one stable minimum to the other. The a_0 meson is always a resonance.

The η' meson mass is always above ω_u up to the point where it reaches the ω_s continuum at higher values of temperature and chemical potential. The f_0 meson is also always unbound with its mass above ω_s .

After the first-order phase transition the pairs π and σ and η and η' degenerate almost immediately. When the a_0 mass (dashed green curve) reaches the mass of the degenerate η and η' pair, the η -meson (solid green curve) decouples from the η' . After this point, the η' and a_0 degenerate and evolve to degenerate with the f_0 meson at high energies while, the η -meson, remains separate from the $[\eta', a_0]$ pair. When the η mass reaches the ω_s continuum its mass increases to asymptotically degenerate with the other mesons.

Regarding the kaons and their chiral partners, right before the first-order phase transition the charge multiplets of the K start to split (see Figure 9 panels (c) and (d)). Before the phase transition only the K mesons are bound while the chiral partners, κ , are resonances. At the first-order phase transition, as expected, there is a discontinuous split of each charge multiplet of both K and κ and every meson is now a resonance, since they all lie above the ω_{us} continuum. As temperature and chemical potential increases, the K^+ and κ^+ mesons start to degenerate, followed by the respective negative pair. For larger energies the charge multiplets of the chiral pair also show tendency to degenerate.

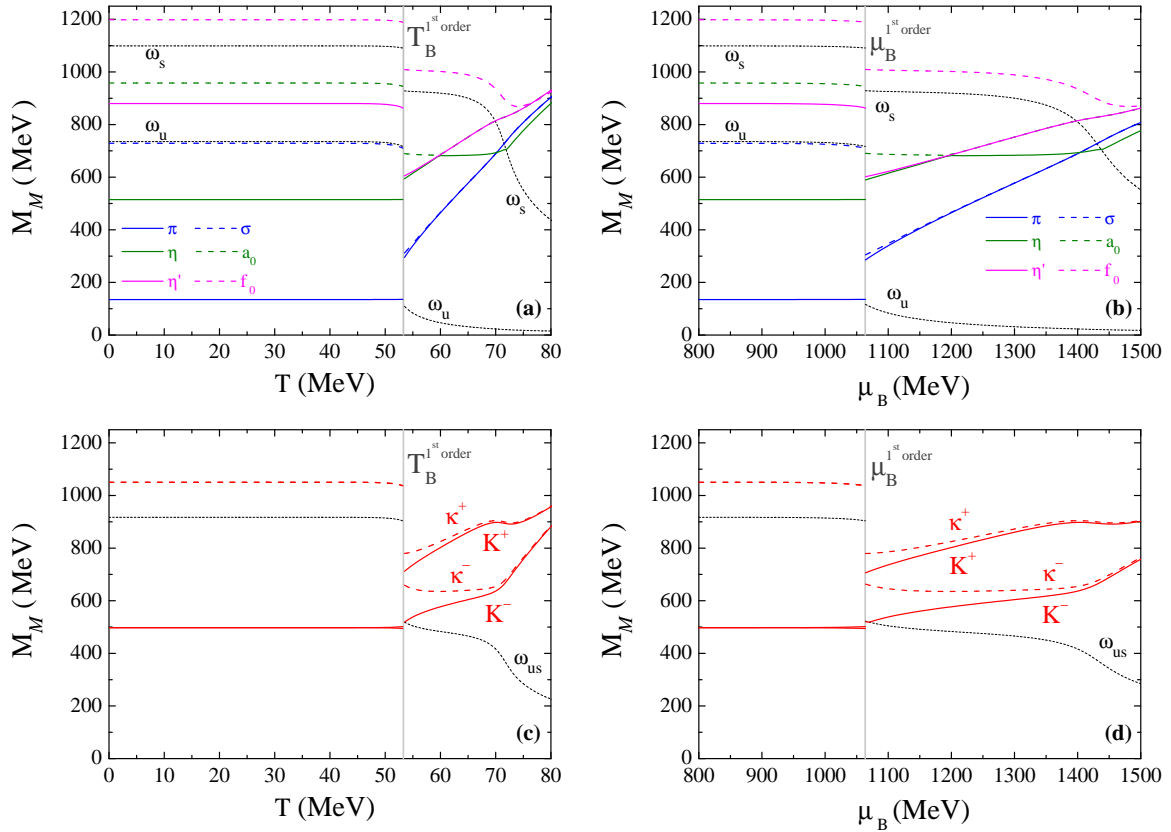


Figure 9. Masses of the pseudoscalar and scalar mesons as function of the temperature (panels (a,c)) and as function of μ_B (panels (b,d)) along the the path $T = 0.05\mu_B$, crossing the first-order region.

4.3.4. Mesons along the Isentropic Trajectory That Passes over the CEP

Previously, the isentropic trajectories relevance was presented, namely the fact that the expansion of the QGP in HIC is accepted to be a hydrodynamic expansion of an ideal fluid and it approximately follows trajectories of constant entropy. This argument motivates the presentation of the behavior of mesons masses as functions of the temperature along the nearest isentropic trajectory of the CEP, $s/\rho_B \approx 5.6$, in Figure 10. There is a substantial difference for the scenario studied in Section 4.3.2 (the path $T = 0.14\mu_B$): the abrupt decrease of the meson masses is not seen. Indeed, in this case, along the isentropic trajectory both, the temperature and the baryonic chemical potential, are varying in such a way that s/ρ_B is held constant. So, the approximation to the CEP is not direct, being the behavior of the mesons masses more smooth in the neighborhood of the CEP. This may be an indication of different critical behavior near the CEP, depending on the direction the CEP is approached in the (T, μ_B) plane. Indeed in [92], the critical exponents in the PNJL model were studied and it was found that their values slightly changed depending on the direction. Nevertheless, from the right panel of Figure 10, we see that the separation between K^+ and K^- is the same (~ 70 MeV) like in Section 4.3.2, as it should.

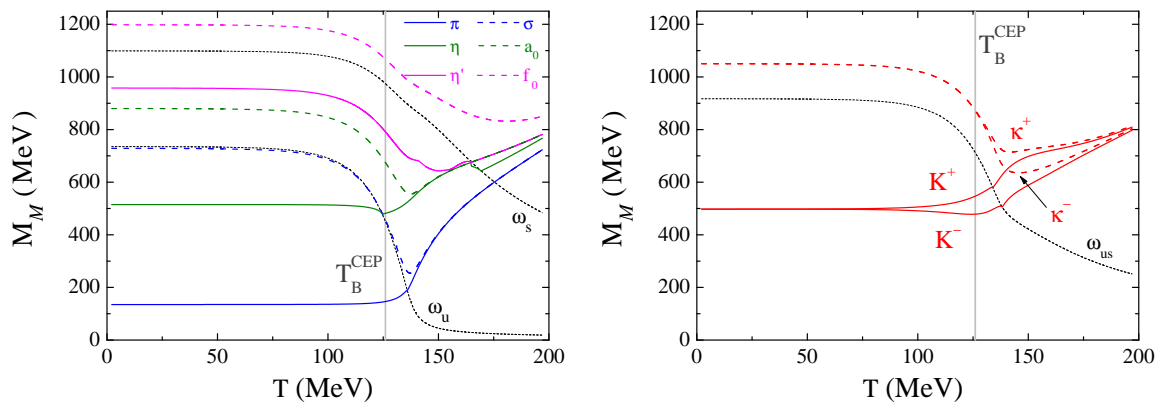


Figure 10. Masses of the pseudoscalar and scalar mesons as function of the temperature (**left panel**) and as function of μ_B (**right panel**) along the the path $T = 0.05\mu_B$, crossing the first-order region.

4.4. Effective Restoration of Chiral Symmetry and Mott Dissociation of π and σ along the Phase Diagram

Since the pion and the sigma mesons dissociate in a $\bar{q}q$ pair, in Figure 11 we represent the respective “Mott lines”. In the region $\mu_B < \mu_B^{CEP}$, the Mott line for σ -meson occurs below chiral crossover, while the correspondent Mott line for π occurs slightly above. It is interesting to note that above $\mu_B \sim \mu_B^{CEP}$ both Mott lines occurs inside the first-order region.

When we use the degeneracy of the π and σ -meson masses as criterion to define the point of the effective restoration of chiral symmetry, we guarantee that all quantities that violate the chiral symmetry are already sufficiently small. We then can draw a line for the effective restoration of chiral symmetry (brown line in Figure 11). For example, when finally $M_\pi = M_\sigma$, the constituent masses of the u and d quarks are already sufficiently close to the respective currents masses values (also the light quark condensates already have a very low values).

5. Conclusions

In this work, we have explored the phase diagram of strongly interacting matter and discussed the scalar-pseudoscalar meson spectrum, with related properties, in connection with the restoration of chiral symmetry and deconfinement for different regions of the phase diagram. We have used the (2 + 1) PNJL model with explicit breaking of the $U_A(1)$ anomaly, which includes flavor mixing, and the coupling of quarks to the Polyakov loop. The PNJL model has proven to be very useful in understanding the underlying concepts of the phase diagram of strongly interacting matter, namely the chiral symmetry breaking and restoration mechanisms. It is also an important tool to study the dynamics of pseudoscalar and scalar mesons with regard to the effective restoration of chiral symmetry.

Some of the presented results have shown a great relevance:

- (i) the survivability of some meson modes, especially the pion, as a bound state after the transition to the QGP (this tendency to a slightly longer survival as bound state is also shown by the behavior of meson-quark coupling constants for π , σ and η mesons);
- (ii) the change of identity between η and η' at finite density for scenarios at lower temperatures;
- (iii) the meson masses change abruptly when choosing a path that passes through the CEP (this can be very important for the signatures of the CEP);
- (iv) in relation to kaons, with the exception of the limiting cases for $T = 0$ and $\mu_B = 0$, a kaon charge splitting before critical temperature/baryonic chemical potential occurs. At CEP and first-order cases, kaons first degenerate with the respective chiral partners and only then with charge multiplet, contrary to the crossover scenario where charge multiplets degenerate first. At the CEP, there is a accentuated splitting for kaons, with K^+ sharply increasing, a splitting that is still pronounced just after the CEP;

- (v) above certain critical values of temperature and chemical potentials ($T_{eff}^\chi, \mu_{B,eff}^\chi$) the masses of the chiral partners [π, σ] will degenerate, meaning that chiral symmetry is effectively restored. All quantities that violate chiral symmetry are guaranteed to be already sufficiently small.

New extensions of the model (e.g., with explicit chiral symmetry breaking interactions that lead to a very good reproduction of the overall characteristics of the LQCD data [153], or with spin-0 and spin-1 $U(3) \times U(3)$ symmetric four-quark interactions to deal with vector–scalar and axial-vector–pseudoscalar transitions [154]) or going beyond the mean-field approximation, by modifying the gap equations due to mesonic fluctuations in the scalar and pseudoscalar channels, can lead the (P)NJL type models to new insights of low energy QCD.

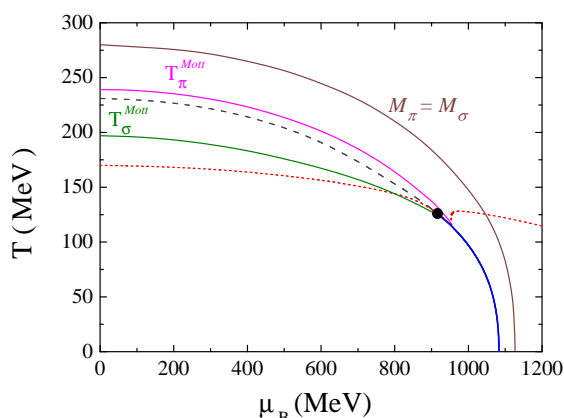


Figure 11. Line of effective restoration of chiral symmetry (brown curve) and the Mott dissociation line for π (magenta) and σ (green) along the $(T - \mu_B)$ -plane.

Author Contributions: Conceptualization, supervision, P.C.; investigation, methodology, formal analysis, writing—original draft preparation, writing—review and editing, P.C. and R.P.

Funding: This work was supported by “Fundação para a Ciência e Tecnologia”, Portugal, under Grant PD/BD/128234/2016 (R.P.).

Acknowledgments: The Authors would like to thank João Moreira for helpful discussions.

Conflicts of Interest: The authors declare no conflict of interest.

Appendix A

The polarization operator for the meson channel M given in Equation (26) in the static limit, $q = 0$ can be calculated to yield:

$$\Pi_{ij}(q_0) = 4 \left((I_1^i + I_1^j) - [q_0^2 - (M_i - M_j)^2] I_2^{ij}(q_0) \right). \tag{A1}$$

where M_i is the effective mass of the quark i . At finite temperature and with two chemical potentials, μ_i and μ_j , the integral I_1^i can be written as:

$$I_1^i(T, \mu_i) = -\frac{N_c}{4\pi^2} \int \frac{p^2 dp}{E_i} (v_i - \bar{v}_i). \tag{A2}$$

The integral I_2^{ij} is given by:

$$I_2^{ij}(q_0, T, \mu_i, \mu_j) = -N_c \int \frac{d^3 p}{(2\pi)^3} \left[\frac{1}{2E_i} \frac{v_i}{(E_i + q_0 - (\mu_i - \mu_j))^2 - E_j^2} - \frac{1}{2E_i} \frac{\bar{v}_i}{(E_i - q_0 + (\mu_i - \mu_j))^2 - E_j^2} + \frac{1}{2E_j} \frac{v_j}{(E_j - q_0 + (\mu_i - \mu_j))^2 - E_i^2} - \frac{1}{2E_j} \frac{\bar{v}_j}{(E_j + q_0 - (\mu_i - \mu_j))^2 - E_i^2} \right]. \tag{A3}$$

Here, E_i is the quasiparticle energy, $E_i = \sqrt{\mathbf{p}^2 + M_i^2}$, μ_i is the chemical potential for the quark i . The distribution functions are given by Equations (23) and (24).

Appendix B

In the $T \rightarrow 0$ limit, the grand canonical potential of the $SU_f(3)$ PNJL and the $SU_f(3)$ NJL model are identical. We can see this by defining the zero temperature limit of Equation (16) as Ω^0 and writing:

$$\begin{aligned}\Omega^0 &= \lim_{T \rightarrow 0} \Omega(T) \\ &= \lim_{T \rightarrow 0} \mathcal{U}(\Phi, \bar{\Phi}; T) + g_s \sum_{i=u,d,s} \langle \bar{q}_i q_i \rangle^2 + 4g_D \langle \bar{q}_u q_u \rangle \langle \bar{q}_d q_d \rangle \langle \bar{q}_s q_s \rangle - 2N_c \sum_{i=u,d,s} \int \frac{d^3 p}{(2\pi)^3} E_i \\ &\quad - 2 \sum_{i=u,d,s} \int \frac{d^3 p}{(2\pi)^3} [\lim_{T \rightarrow 0} \mathcal{F}(\mathbf{p}, T, \mu_i) + \lim_{T \rightarrow 0} \mathcal{F}^*(\mathbf{p}, T, \mu_i)].\end{aligned}\quad (\text{A4})$$

The Polyakov loop potential, $\mathcal{U}(\Phi, \bar{\Phi}; T)$, as defined in Equation (10), vanishes in this limit. The limits of the thermal functions (17) and (18) are given by:

$$\lim_{T \rightarrow 0} \mathcal{F}(T, \mu_i) = 3(\mu_i - E_i) \theta(E_i - \mu_i), \quad (\text{A5})$$

$$\lim_{T \rightarrow 0} \mathcal{F}^*(T, \mu_i) = 0. \quad (\text{A6})$$

where $\theta(E_i - \mu_i)$ is the Heaviside step function. One can define the Fermi momentum of the quark of flavor i as:

$$\lambda_{F_i} = \sqrt{\mu_i^2 - M_i^2}. \quad (\text{A7})$$

The grand canonical potential can then be written as:

$$\Omega^0 = g_s \sum_{i=u,d,s} \langle \bar{q}_i q_i \rangle^2 + 4g_D \langle \bar{q}_u q_u \rangle \langle \bar{q}_d q_d \rangle \langle \bar{q}_s q_s \rangle - \frac{N_c}{\pi^2} \sum_{i=u,d,s} \int_{\lambda_{F_i}}^{\Lambda} dp p^2 E_i - \sum_{i=u,d,s} \mu_i \frac{\lambda_{F_i}^3}{\pi^2}. \quad (\text{A8})$$

The i -quark density is:

$$\rho_i = \frac{\lambda_{F_i}^3}{\pi^2}. \quad (\text{A9})$$

Applying the stationary conditions yields the respective i -quark condensate,

$$\langle \bar{q}_i q_i \rangle = -\frac{N_c}{\pi^2} \int_{\lambda_{F_i}}^{\Lambda} dp p^2 \frac{M_i}{E_i}. \quad (\text{A10})$$

These set of equations, which define the $SU_f(3)$ PNJL in this limit, are identical to those defining the $SU_f(3)$ NJL at zero temperature.

References

1. Nambu, Y.; Jona-Lasinio, G. Dynamical Model of Elementary Particles Based on an Analogy with Superconductivity. I. *Phys. Rev.* **1961**, *122*, 345–358. [[CrossRef](#)]
2. Nambu, Y.; Jona-Lasinio, G. Dynamical Model of Elementary Particles Based on an Analogy with Superconductivity. II. *Phys. Rev.* **1961**, *124*, 246–254. [[CrossRef](#)]
3. Vaks, V.G.; Larkin, A.I. On the application of the methods of superconductivity theory to the problem of the masses of elementary particles. *Sov. Phys. JETP* **1961**, *13*, 192–193.
4. Eguchi, T. A new approach to collective phenomena in superconductivity models. *Phys. Rev.* **1976**, *D14*, 2755. [[CrossRef](#)]
5. Kikkawa, K. Quantum corrections in superconductor models. *Prog. Theor. Phys.* **1976**, *56*, 947. [[CrossRef](#)]

6. Volkov, M.K.; Ebert, D. Four-quark interactions as a common source of the vector meson dominance and Sigma model. *Yad. Fiz.* **1982**, *36*, 1265–1277. (In Russian)
7. Ebert, D.; Volkov, M.K. Composite Meson Model with Vector Dominance Based on U(2) Invariant Four Quark Interactions. *Z. Phys.* **1983**, *C16*, 205. [[CrossRef](#)]
8. Volkov, M.K. Meson Lagrangians in a Superconductor Quark Model. *Ann. Phys.* **1984**, *157*, 282–303. [[CrossRef](#)]
9. Vogl, U.; Weise, W. The Nambu and Jona Lasinio model: Its implications for hadrons and nuclei. *Prog. Part. Nucl. Phys.* **1991**, *27*, 195–272. [[CrossRef](#)]
10. Kunihiro, T.; Hatsuda, T. Effects of Flavor Mixing Induced by Axial Anomaly on the Quark Condensates and Meson Spectra. *Phys. Lett.* **1988**, *B206*, 385–390. [[CrossRef](#)]
11. Bernard, V.; Jaffe, R.L.; Meissner, U.G. Strangeness Mixing and Quenching in the Nambu-Jona-Lasinio Model. *Nucl. Phys.* **1988**, *B308*, 753–790. [[CrossRef](#)]
12. Reinhardt, H.; Alkofer, R. Instanton Induced Flavor Mixing in Mesons. *Phys. Lett.* **1988**, *B207*, 482–488. [[CrossRef](#)]
13. Kobayashi, M.; Maskawa, T. Chiral symmetry and eta-x mixing. *Prog. Theor. Phys.* **1970**, *44*, 1422–1424. [[CrossRef](#)]
14. Kobayashi, M.; Kondo, H.; Maskawa, T. Symmetry breaking of the chiral $u(3) \times u(3)$ and the quark model. *Prog. Theor. Phys.* **1971**, *45*, 1955–1959. [[CrossRef](#)]
15. Hooft, G.T. Computation of the Quantum Effects Due to a Four-Dimensional Pseudoparticle. *Phys. Rev.* **1976**, *D14*, 3432–3450. [[CrossRef](#)]
16. Hooft, G.T. How Instantons Solve the U(1) Problem. *Phys. Rep.* **1986**, *142*, 357–387. [[CrossRef](#)]
17. Adler, S.L. Axial vector vertex in spinor electrodynamics. *Phys. Rev.* **1969**, *177*, 2426–2438. [[CrossRef](#)]
18. Bell, J.S.; Jackiw, R. A PCAC puzzle: $\pi^0 \rightarrow \gamma\gamma$ in the σ model. *Nuovo Cim.* **1969**, *A60*, 47–61. [[CrossRef](#)]
19. Klevansky, S.P. The Nambu-Jona-Lasinio model of quantum chromodynamics. *Rev. Mod. Phys.* **1992**, *64*, 649–708. [[CrossRef](#)]
20. Hatsuda, T.; Kunihiro, T. QCD phenomenology based on a chiral effective Lagrangian. *Phys. Rept.* **1994**, *247*, 221–367. [[CrossRef](#)]
21. Buballa, M. NJL model analysis of quark matter at large density. *Phys. Rept.* **2005**, *407*, 205–376. [[CrossRef](#)]
22. Osipov, A.A.; Hiller, B.; da Providencia, J. Multi-quark interactions with a globally stable vacuum. *Phys. Lett.* **2006**, *B634*, 48–54. [[CrossRef](#)]
23. Osipov, A.A.; Hiller, B.; Blin, A.H.; da Providencia, J. Effects of eight-quark interactions on the hadronic vacuum and mass spectra of light mesons. *Ann. Phys.* **2007**, *322*, 2021–2054. [[CrossRef](#)]
24. Osipov, A.A.; Hiller, B.; Moreira, J.; Blin, A.H. OZI violating eight-quark interactions as a thermometer for chiral transitions. *Phys. Lett.* **2008**, *B659*, 270–274. [[CrossRef](#)]
25. Fukushima, K. Chiral effective model with the Polyakov loop. *Phys. Lett.* **2004**, *B591*, 277–284. [[CrossRef](#)]
26. Ratti, C.; Thaler, M.A.; Weise, W. Phases of QCD: Lattice thermodynamics and a field theoretical model. *Phys. Rev.* **2006**, *D73*, 014019. [[CrossRef](#)]
27. Hansen, H.; Alberico, W.; Beraudo, A.; Molinari, A.; Nardi, M.; Ratti, C. Mesonic correlation functions at finite temperature and density in the Nambu-Jona-Lasinio model with a Polyakov loop. *Phys. Rev.* **2007**, *D75*, 065004. [[CrossRef](#)]
28. Meisinger, P.N.; Ogilvie, M.C. Chiral symmetry restoration and Z_N symmetry. *Phys. Lett.* **1996**, *B379*, 163–168. [[CrossRef](#)]
29. Pisarski, R.D. Quark-gluon plasma as a condensate of SU(3) Wilson lines. *Phys. Rev.* **2000**, *D62*, 111501. [[CrossRef](#)]
30. Pisarski, R.D. Notes on the Deconfining Phase Transition. *arXiv* **2002**, arXiv:hep-ph/0203271.
31. Meisinger, P.N.; Miller, T.R.; Ogilvie, M.C. Phenomenological equations of state for the quark-gluon plasma. *Phys. Rev.* **2002**, *D65*, 034009. [[CrossRef](#)]
32. Mocsy, A.; Sannino, F.; Tuominen, K. Confinement versus Chiral Symmetry. *Phys. Rev. Lett.* **2004**, *92*, 182302. [[CrossRef](#)]
33. Hatsuda, T.; Kunihiro, T. Character Changes of Pion and Sigma Meson at Finite Temperature. *Phys. Lett.* **1987**, *B185*, 304. [[CrossRef](#)]
34. Bernard, V.; Meissner, U.G.; Zahed, I. Properties of the Scalar σ Meson at Finite Density. *Phys. Rev. Lett.* **1987**, *59*, 966. [[CrossRef](#)]

35. Bernard, V.; Meissner, U.G.; Zahed, I. Decoupling of the Pion at Finite Temperature and Density. *Phys. Rev.* **1987**, *D36*, 819. [[CrossRef](#)]
36. Bernard, V.; Meissner, U.G. Properties of Vector and Axial Vector Mesons from a Generalized Nambu-Jona-Lasinio Model. *Nucl. Phys.* **1988**, *A489*, 647–670. [[CrossRef](#)]
37. Klimt, S.; Lutz, M.F.M.; Vogl, U.; Weise, W. Generalized SU(3) Nambu-Jona-Lasinio Model. Part 1. Mesonic Modes. *Nucl. Phys.* **1990**, *A516*, 429–468. [[CrossRef](#)]
38. Vogl, U.; Lutz, M.F.M.; Klimt, S.; Weise, W. Generalized SU(3) Nambu-Jona-Lasinio Model. Part 2. From Current to Constituent Quarks. *Nucl. Phys.* **1990**, *A516*, 469–495. [[CrossRef](#)]
39. Lutz, M.F.M.; Klimt, S.; Weise, W. Meson properties at finite temperature and baryon density. *Nucl. Phys.* **1992**, *A542*, 521–558. [[CrossRef](#)]
40. Ruivo, M.C.; de Sousa, C.A.; Hiller, B.; Blin, A.H. Medium effects on meson properties. *Nucl. Phys.* **1994**, *A575*, 460–476. [[CrossRef](#)]
41. Ruivo, M.C.; de Sousa, C.A. Kaon properties at finite baryonic density: A nonperturbative approach. *Phys. Lett.* **1996**, *B385*, 39–44. [[CrossRef](#)]
42. de Sousa, C.A.; Ruivo, M.C. Fermi sea effects on pion and kaon properties in the Nambu-Jona-Lasinio model. *Nucl. Phys.* **1997**, *A625*, 713–728. [[CrossRef](#)]
43. Ruivo, M.C.; de Sousa, C.A.; Providencia, C. Kaons in a hot and flavor-asymmetric medium. *Nucl. Phys.* **1999**, *A651*, 59–70. [[CrossRef](#)]
44. Bhattacharyya, A.; Ghosh, S.K.; Raha, S. Pion and kaon dissociation in hot quark medium. *Mod. Phys. Lett.* **1999**, *A14*, 621–630. [[CrossRef](#)]
45. Rehberg, P.; Klevansky, S.; Hufner, J. Hadronization in the SU(3) Nambu-Jona-Lasinio model. *Phys. Rev.* **1996**, *C53*, 410–429. [[CrossRef](#)]
46. Costa, P.; Ruivo, M.C.; de Sousa, C.A.; Kalinovsky, Yu.L. Effective restoration of the $U_A(1)$ symmetry with temperature and density. *Phys. Rev.* **2004**, *D70*, 116013. [[CrossRef](#)]
47. Costa, P.; Ruivo, M.C.; de Sousa, C.A.; Kalinovsky, Yu.L. Analysis of the $U_A(1)$ symmetry-breaking and restoration effects on scalar-pseudoscalar spectrum. *Phys. Rev.* **2005**, *D71*, 116002. [[CrossRef](#)]
48. Blanquier, E. Standard particles in the SU(3) Nambu-Jona-Lasinio model and the Polyakov-NJL model. *J. Phys.* **2011**, *G38*, 105003. [[CrossRef](#)]
49. Blanquier, E. Hadronization within a Nambu-Jona-Lasinio model with a Polyakov loop. *Phys. Rev.* **2014**, *C89*, 065204. [[CrossRef](#)]
50. Blaschke, D.; Dubinin, A.; Radzhabov, A.; Wergieluk, A. Mott dissociation of pions and kaons in hot, dense quark matter. *Phys. Rev.* **2017**, *D96*, 094008. [[CrossRef](#)]
51. Costa, P.; Ruivo, M.C.; de Sousa, C.A.; Hansen, H.; Alberico, W.M. Scalar-pseudoscalar meson behavior and restoration of symmetries in SU(3) PNJL model. *Phys. Rev.* **2009**, *D79*, 116003. [[CrossRef](#)]
52. Blanquier, E. Cross sections in the Polyakov-Nambu-Jona-Lasinio model: Study of reactions involving quarks, antiquarks, mesons, diquarks and baryons. *J. Phys.* **2012**, *G39*, 105003. [[CrossRef](#)]
53. Dubinin, A.; Blaschke, D.; Kalinovsky, Yu.L. Pion and sigma meson dissociation in a modified NJL model at finite temperature. *Acta Phys. Polon. Suppl.* **2014**, *7*, 215–223. [[CrossRef](#)]
54. Gottfried, F.O.; Klevansky, S.P. Thermodynamics of open and hidden charmed mesons within the NJL model. *Phys. Lett.* **1992**, *B286*, 221–224. [[CrossRef](#)]
55. Blaschke, D.; Burau, G.; Kalinovsky, Yu. L.; Yudichev, V.L. Chiral symmetry restoration and anomalous J/ψ suppression. *Prog. Theor. Phys. Suppl.* **2003**, *149*, 182–189. [[CrossRef](#)]
56. Guo, X.Y.; Chen, X.L.; Deng, W.Z. The Heavy mesons in Nambu-Jona-Lasinio model. *Chin. Phys.* **2013**, *C37*, 033102. [[CrossRef](#)]
57. Caramés, T.; Fontoura, C.; Krein, G.; Tsushima, K.; Vijande, J.; Valcarce, A. Hadronic molecules with a \bar{D} meson in a medium. *Phys. Rev.* **2016**, *D94*, 034009. [[CrossRef](#)]
58. Blaschke, D.; Costa, P.; Kalinovsky, Yu. L. D mesons at finite temperature and density in the PNJL model. *Phys. Rev.* **2012**, *D85*, 034005. [[CrossRef](#)]
59. Cabibbo, N.; Parisi, G. Exponential Hadronic Spectrum and Quark Liberation. *Phys. Lett.* **1975**, *59B*, 67–69. [[CrossRef](#)]
60. Brambilla, N.; Eidelman, S.; Foka, P.; Gardner, S.; Kronfeld, A.S.; Alford, M.G.; Alkofer, R.; Butenschoen, M.; Cohen, T.D.; Erdmenger, J.; et al. QCD and Strongly Coupled Gauge Theories: Challenges and Perspectives. *Eur. Phys. J.* **2014**, *C74*, 2981. [[CrossRef](#)]

61. Halasz, A.M.; Jackson, A.D.; Shrock, R.E.; Stephanov, M.A.; Verbaarschot, J.J.M. On the phase diagram of QCD. *Phys. Rev.* **1998**, *D58*, 096007. [[CrossRef](#)]
62. Gupta, S.; Luo, X.; Mohanty, B.; Ritter, H.G.; Xu, N. Scale for the Phase Diagram of Quantum Chromodynamics. *Science* **2011**, *332*, 1525–1528. [[CrossRef](#)]
63. Schmidt, C.; Sharma, S. The phase structure of QCD. *J. Phys.* **2017**, *G44*, 104002. [[CrossRef](#)]
64. Seiler, E. Status of Complex Langevin. *EPJ Web Conf.* **2018**, *175*, 01019. [[CrossRef](#)]
65. Roberts, C.D.; Williams, A.G. Dyson-Schwinger equations and their application to hadronic physics. *Prog. Part. Nucl. Phys.* **1994**, *33*, 477–575. [[CrossRef](#)]
66. Roberts, C.D. Strong QCD and Dyson-Schwinger Equations. *IRMA Lect. Math. Theor. Phys.* **2015**, *21*, 355–458.
67. Fischer, C.S. QCD at finite temperature and chemical potential from Dyson—Schwinger equations. *Prog. Part. Nucl. Phys.* **2019**, *105*, 1–60. [[CrossRef](#)]
68. Borsanyi, S.; Fodor, Z.; Hoelbling, C.; Katz, S.D.; Krieg, S.; Ratti, C.; Szabo, K.K. Is there still any Tc mystery in lattice QCD? Results with physical masses in the continuum limit III. *JHEP* **2010**, *9*, 073. [[CrossRef](#)]
69. Bazavov, A.; others. Equation of state in (2 + 1)-flavor QCD. *Phys. Rev.* **2014**, *D90*, 094503. [[CrossRef](#)]
70. Fodor, Z.; Katz, S. Critical point of QCD at finite T and mu, lattice results for physical quark masses. *JHEP* **2004**, *0404*, 050. [[CrossRef](#)]
71. Fischer, C.S.; Fister, L.; Luecker, J.; Pawłowski, J.M. Polyakov loop potential at finite density. *Phys. Lett.* **2014**, *B732*, 273–277. [[CrossRef](#)]
72. Fischer, C.S.; Luecker, J.; Welzbacher, C.A. Phase structure of three and four flavor QCD. *Phys. Rev.* **2014**, *D90*, 034022. [[CrossRef](#)]
73. Adamczyk, L.; Adkins, J.K.; Agakishiev, G.; Aggarwal, M.M.; Ahammed, Z.; Alekseev, I.; Alford, J.; Anson, C.D.; Aparin, A.; Arkhipkin, D.; et al. Beam energy dependence of moments of the net-charge multiplicity distributions in Au + Au collisions at RHIC. *Phys. Rev. Lett.* **2014**, *113*, 092301. [[CrossRef](#)]
74. Adamczyk, L.; Adams, J.R.; Adkins, J.K.; Agakishiev, G.; Aggarwal, M.M.; Ahammed, Z.; Ajitanand, N.N.; Alekseev, I.; Anderson, D.M.; Aoyama, R.; et al. Collision Energy Dependence of Moments of Net-Kaon Multiplicity Distributions at RHIC. *Phys. Lett.* **2018**, *B785*, 551–560. [[CrossRef](#)]
75. Adamczyk, L.; Adkins, J.K.; Agakishiev, G.; Aggarwal, M.M.; Ahammed, Z.; Ajitanand, N.N.; Alekseev, I.; Anderson, D.M.; Aoyama, R.; Aparin, A.; et al. Bulk Properties of the Medium Produced in Relativistic Heavy-Ion Collisions from the Beam Energy Scan Program. *Phys. Rev.* **2017**, *C96*, 044904. [[CrossRef](#)]
76. Aduszkiewicz, A.; Ali, Y.; Andronov, E.; Antičić, T.; Antoniou, N.; Baatar, B.; Bay, F.; Blondel, A.; Blücher, J.; Bogomilov, M.; et al. Multiplicity and transverse momentum fluctuations in inelastic proton—Proton interactions at the CERN Super Proton Synchrotron. *Eur. Phys. J.* **2016**, *C76*, 635. [[CrossRef](#)]
77. Grebieszko, K. New results on fluctuations and correlations from the NA61/SHINE experiment at the CERN SPS. *PoS* **2017**, *EPS-HEP2017*, 167. [[CrossRef](#)]
78. Sako, H.; Chujo, T.; Gunji, T.; Harada, H.; Imai, K.; Kaneta, M.; Kinsho, M.; Liu, Y.; Nagamiya, S.; Nishio, K.; et al. Towards the heavy-ion program at J-PARC. *Nucl. Phys. A* **2014**, *931*, 1158–1162. [[CrossRef](#)]
79. Ablyazimov, T.; Abuhoza, A.; Adak, R.P.; Adamczyk, M.; Agarwal, K.; Aggarwal, M.M.; Ahammed, Z.; Ahmad, F.; Ahmad, N.; Ahmad, S.; et al. Challenges in QCD matter physics—The scientific programme of the Compressed Baryonic Matter experiment at FAIR. *Eur. Phys. J.* **2017**, *A53*, 60. [[CrossRef](#)]
80. Blaschke, D.; Aichelin, J.; Bratkovskaya, E.; Friese, V.; Gazdzicki, M.; Randrup, J.; Rogachevsky, O.; Teryaev, O.; Toneev, V. Topical issue on Exploring Strongly Interacting Matter at High Densities—NICA White Paper. *Eur. Phys. J. A* **2016**, *52*, 267. [[CrossRef](#)]
81. Akiba, Y.; Angerami, A.; Caines, H.; Frawley, A.; Heinz, U.; Jacak, B.; Jia, J.; Lappi, T.; Li, W.; Majumder, A.; et al. The Hot QCD White Paper: Exploring the Phases of QCD at RHIC and the LHC *arXiv* **2015**, arXiv:1502.02730.
82. Asakawa, M.; Yazaki, K. Chiral Restoration at Finite Density and Temperature. *Nucl. Phys.* **1989**, *A504*, 668–684. [[CrossRef](#)]
83. Schwarz, T.M.; Klevansky, S.P.; Papp, G. The Phase diagram and bulk thermodynamical quantities in the NJL model at finite temperature and density. *Phys. Rev.* **1999**, *C60*, 055205. [[CrossRef](#)]
84. Zhuang, P.; Huang, M.; Yang, Z. Density effect on hadronization of a quark plasma. *Phys. Rev.* **2000**, *C62*, 054901. [[CrossRef](#)]
85. Scavenius, O.; Mocsy, A.; Mishustin, I.N.; Rischke, D.H. Chiral phase transition within effective models with constituent quarks. *Phys. Rev.* **2001**, *C64*, 045202. [[CrossRef](#)]

86. Fujii, H. Scalar density fluctuation at critical end point in NJL model. *Phys. Rev.* **2003**, *D67*, 094018. [[CrossRef](#)]
87. Biguet, A.; Hansen, H.; Brugière, T.; Costa, P.; Borgnat, P. Sensitivity of predictions in an effective model—Application to the chiral critical end point position in the Nambu–Jona-Lasinio model. *Eur. Phys. J.* **2015**, *A51*, 121. [[CrossRef](#)]
88. Mishustin, I.N.; Satarov, L.M.; Stoecker, H.; Greiner, W. Unusual bound states of quark matter within the NJL model. *Phys. Rev.* **2000**, *C62*, 034901. [[CrossRef](#)]
89. Costa, P.; de Sousa, C.A.; Ruivo, M.C.; Kalinovsky, Y.L. The QCD critical end point in the SU(3) Nambu–Jona-Lasinio model. *Phys. Lett.* **2007**, *B647*, 431–435. [[CrossRef](#)]
90. Costa, P.; Ruivo, M.C.; de Sousa, C.A. Thermodynamics and critical behavior in the Nambu–Jona-Lasinio model of QCD. *Phys. Rev.* **2008**, *D77*, 096001. [[CrossRef](#)]
91. Fu, W.J.; Zhang, Z.; Liu, Y.X. 2 + 1 Flavor Polyakov–Nambu–Jona-Lasinio Model at Finite Temperature and Nonzero Chemical Potential. *Phys. Rev.* **2008**, *D77*, 014006. [[CrossRef](#)]
92. Costa, P.; de Sousa, C.A.; Ruivo, M.C.; Hansen, H. The QCD critical end point in the PNJL model. *EPL* **2009**, *86*, 31001. [[CrossRef](#)]
93. Costa, P.; Ruivo, M.C.; de Sousa, C.A.; Hansen, H. Phase diagram and critical properties within an effective model of QCD: the Nambu–Jona-Lasinio model coupled to the Polyakov loop. *Symmetry* **2010**, *2*, 1338–1374. [[CrossRef](#)]
94. Friesen, A.V.; Kalinovsky, Yu.L.; Toneev, V.D. Vector interaction effect on thermodynamics and phase structure of QCD matter. *Int. J. Mod. Phys.* **2015**, *A30*, 1550089. [[CrossRef](#)]
95. Torres-Rincon, J.M.; Aichelin, J. Equation of state of a quark-meson mixture in the improved Polyakov–Nambu–Jona-Lasinio model at finite chemical potential. *Phys. Rev.* **2017**, *C96*, 045205. [[CrossRef](#)]
96. Schertler, K.; Leupold, S.; Schaffner-Bielich, J. Neutron stars and quark phases in the NJL model. *Phys. Rev.* **1999**, *C60*, 025801. [[CrossRef](#)]
97. Hanauske, M.; Satarov, L.M.; Mishustin, I.N.; Stoecker, H.; Greiner, W. Strange quark stars within the Nambu–Jona-Lasinio model. *Phys. Rev.* **2001**, *D64*, 043005. [[CrossRef](#)]
98. Buballa, M.; Neumann, F.; Oertel, M.; Shovkovy, I. Quark mass effects on the stability of hybrid stars. *Phys. Lett.* **2004**, *B595*, 36–43. [[CrossRef](#)]
99. Menezes, D.P.; Providencia, C. Warm stellar matter with deconfinement: Application to compact stars. *Phys. Rev.* **2003**, *C68*, 035804. [[CrossRef](#)]
100. Lenzi, C.H.; Schneider, A.S.; Providencia, C.; Marinho, R.M. Compact stars with a quark core within NJL model. *Phys. Rev.* **2010**, *C82*, 015809. [[CrossRef](#)]
101. Bonanno, L.; Sedrakian, A. Composition and stability of hybrid stars with hyperons and quark color-superconductivity. *Astron. Astrophys.* **2012**, *539*, A16. [[CrossRef](#)]
102. Pereira, R.C.; Costa, P.; Providência, C. Two-solar-mass hybrid stars: A two model description with the Nambu–Jona-Lasinio quark model. *Phys. Rev.* **2016**, *D94*, 094001. [[CrossRef](#)]
103. Menezes, D.P.; Benghi Pinto, M.; Avancini, S.S.; Perez Martinez, A.; Providencia, C. Quark matter under strong magnetic fields in the Nambu–Jona-Lasinio Model. *Phys. Rev.* **2009**, *C79*, 035807. [[CrossRef](#)]
104. Ferreira, M.; Costa, P.; Menezes, D.P.; Providência, C.; Scoccola, N. Deconfinement and chiral restoration within the SU(3) Polyakov–Nambu–Jona-Lasinio and entangled Polyakov–Nambu–Jona-Lasinio models in an external magnetic field. *Phys. Rev.* **2014**, *D89*, 016002. [[CrossRef](#)]
105. Costa, P.; Ferreira, M.; Hansen, H.; Menezes, D.P.; Providência, C. Phase transition and critical end point driven by an external magnetic field in asymmetric quark matter. *Phys. Rev.* **2014**, *D89*, 056013. [[CrossRef](#)]
106. Ferreira, M.; Costa, P.; Lourenço, O.; Frederico, T.; Providência, C. Inverse magnetic catalysis in the (2 + 1)-flavor Nambu–Jona-Lasinio and Polyakov–Nambu–Jona-Lasinio models. *Phys. Rev.* **2014**, *D89*, 116011. [[CrossRef](#)]
107. Costa, P.; Ferreira, M.; Menezes, D.P.; Moreira, J.; Providência, C. Influence of the inverse magnetic catalysis and the vector interaction in the location of the critical end point. *Phys. Rev.* **2015**, *D92*, 036012. [[CrossRef](#)]
108. Ferreira, M.; Costa, P.; Providência, C. Multiple critical endpoints in magnetized three flavor quark matter. *Phys. Rev.* **2018**, *D97*, 014014. [[CrossRef](#)]
109. Ferreira, M.; Costa, P.; Providência, C. Presence of a critical endpoint in the QCD phase diagram from the net-baryon number fluctuations. *Phys. Rev.* **2018**, *D98*, 034006. [[CrossRef](#)]

110. Roessner, S.; Ratti, C.; Weise, W. Polyakov loop, diquarks and the two-flavour phase diagram. *Phys. Rev.* **2007**, *D75*, 034007. [[CrossRef](#)]
111. Fukushima, K. Phase diagrams in the three-flavor Nambu-Jona-Lasinio model with the Polyakov loop. *Phys. Rev.* **2008**, *D77*, 114028. [[CrossRef](#)]
112. Ejiri, S.; Iwasaki, Y.; Kanaya, K. Nonperturbative determination of anisotropy coefficients in lattice gauge theories. *Phys. Rev.* **1998**, *D58*, 094505. [[CrossRef](#)]
113. Boyd, G.; Engels, J.; Karsch, F.; Laermann, E.; Legeland, C.; Lutgemeier, M.; Petersson, B. Thermodynamics of SU(3) lattice gauge theory. *Nucl. Phys.* **1996**, *B469*, 419–444. [[CrossRef](#)]
114. Kaczmarek, O.; Karsch, F.; Petreczky, P.; Zantow, F. Heavy quark anti-quark free energy and the renormalized Polyakov loop. *Phys. Lett.* **2002**, *B543*, 41–47. [[CrossRef](#)]
115. Ruivo, M.C.; Costa, P.; de Sousa, C.A.; Kalinovsky, Yu, L. Effective restoration of chiral and axial symmetries at finite temperature and density. *J. Phys.* **2005**, *G31*, S1183–S1186. [[CrossRef](#)]
116. Costa, P.; Ruivo, M.C.; Kalinovsky, Yu.L.; de Sousa, C.A. Pseudoscalar mesons in hot, dense matter. *Phys. Rev.* **2004**, *C70*, 025204. [[CrossRef](#)]
117. Bazavov, A.; Ding, H.T.; Hegde, P.; Kaczmarek, O.; Karsch, F.; Laermann, E.; Mukherjee, S.; Petreczky, P.; Schmidt, C.; Smith, D.; et al. Freeze-out Conditions in Heavy Ion Collisions from QCD Thermodynamics. *Phys. Rev. Lett.* **2012**, *109*, 192302. [[CrossRef](#)]
118. Kapusta, J.I.; Gale, C. *Finite-Temperature Field Theory: Principles and Applications*; Cambridge Monographs on Mathematical Physics; Cambridge University Press: Cambridge, UK, 2011. [[CrossRef](#)]
119. Van den Bossche, B. The Three Flavor A Scaled Nambu-Jona-Lasinio Model. Ph.D. Thesis, Université de Liège, Liège, Belgium, 1996.
120. Pauli, W.; Villars, F. On the Invariant regularization in relativistic quantum theory. *Rev. Mod. Phys.* **1949**, *21*, 434–444, 10.1103/RevModPhys.21.434. [[CrossRef](#)]
121. Schuren, C.; Doring, F.; Ruiz Arriola, E.; Goetze, K. Vector mesons in the Nambu-Jona-Lasinio model. *Nucl. Phys.* **1993**, *A565*, 687–739. [[CrossRef](#)]
122. Dmitrasinovic, V.; Schulze, H.J.; Tegen, R.; Lemmer, R.H. Chirally symmetric O (1/N(c corrections to the Nambu-Jona-Lasinio model. *Ann. Phys.* **1995**, *238*, 332–369. [[CrossRef](#)]
123. Schwinger, J.S. On gauge invariance and vacuum polarization. *Phys. Rev.* **1951**, *82*, 664–679. [[CrossRef](#)]
124. Ripka, G. *Quarks Bound by Chiral Fields: The Quark-Structure of the Vacuum and of Light Mesons and Baryons*; Oxford Studies in Nuclear Physics; Clarendon Press: Oxford, UK, 1997.
125. Van den Bossche, B. The Three flavor A scaled Nambu-Jona-Lasinio model. In Proceedings of the Research Workshop on Deconfinement at Finite Temperature and Density, Dubna, Russia, 1–25 October 1997.
126. Costa, P.; Ruivo, M.C.; de Sousa, C.A. Effects of the regularization on the restoration of chiral and axial symmetries. *Phys. Rev.* **2008**, *D77*, 096009. [[CrossRef](#)]
127. Costa, P.; Hansen, H.; Ruivo, M.C.; de Sousa, C.A. How parameters and regularization affect the PNJL model phase diagram and thermodynamic quantities. *Phys. Rev.* **2010**, *D81*, 016007. [[CrossRef](#)]
128. Bratovic, N.M.; Hatsuda, T.; Weise, W. Role of Vector Interaction and Axial Anomaly in the PNJL Modeling of the QCD Phase Diagram. *Phys. Lett.* **2013**, *B719*, 131–135. [[CrossRef](#)]
129. Moreira, J.; Hiller, B.; Osipov, A.A.; Blin, A.H. Thermodynamic potential with correct asymptotics for PNJL model. *Int. J. Mod. Phys.* **2012**, *A27*, 1250060. [[CrossRef](#)]
130. Karsch, F. Lattice QCD at high temperature and density. *Lect. Notes Phys.* **2002**, *583*, 209–249. [[CrossRef](#)]
131. Borsanyi, S.; Endrodi, G.; Fodor, Z.; Katz, S.D.; Szabo, K.K. Precision SU(3) lattice thermodynamics for a large temperature range. *JHEP* **2012**, *07*, 056. [[CrossRef](#)]
132. Schaefer, B.J.; Pawłowski, J.M.; Wambach, J. The Phase Structure of the Polyakov-Quark-Meson Model. *Phys. Rev.* **2007**, *D76*, 074023. [[CrossRef](#)]
133. Kaczmarek, O. Screening at finite temperature and density. *PoS* **2007**, *CPOD07*, 043.
134. Aoki, Y.; Borsanyi, S.; Durr, S.; Fodor, Z.; Katz, S.D.; Krieg, S.; Szabo, K.K. The QCD transition temperature: results with physical masses in the continuum limit II. *JHEP* **2009**, *6*, 88. [[CrossRef](#)]
135. Bluhm, M.; Kampfer, B.; Schulze, R.; Seipt, D.; Heinz, U. A family of equations of state based on lattice QCD: Impact on flow in ultrarelativistic heavy-ion collisions. *Phys. Rev.* **2007**, *C76*, 034901. [[CrossRef](#)]
136. Costa, P. Influence of the vector interaction and an external magnetic field on the isentropes near the chiral critical end point. *Phys. Rev.* **2016**, *D93*, 114035. [[CrossRef](#)]

137. Ejiri, S.; Karsch, F.; Laermann, E.; Schmidt, C. The isentropic equation of state of 2-flavor QCD. *Phys. Rev.* **2006**, *D73*, 054506. [[CrossRef](#)]
138. Borsanyi, S.; Endrodi, G.; Fodor, Z.; Katz, S.D.; Krieg, S.; Ratti, C.; Szabo, K.K. QCD equation of state at nonzero chemical potential: continuum results with physical quark masses at order μ^2 . *JHEP* **2012**, *8*, 053. [[CrossRef](#)]
139. Nonaka, C.; Asakawa, M. Hydrodynamical evolution near the QCD critical end point. *Phys. Rev.* **2005**, *C71*, 044904. [[CrossRef](#)]
140. Fukushima, K. Isentropic thermodynamics in the PNJL model. *Phys. Rev.* **2009**, *D79*, 074015. [[CrossRef](#)]
141. Kahara, T.; Tuominen, K. Degrees of freedom and the phase transitions of two flavor QCD. *Phys. Rev.* **2008**, *D78*, 034015. [[CrossRef](#)]
142. Nakano, E.; Schaefer, B.J.; Stokic, B.; Friman, B.; Redlich, K. Fluctuations and isentropes near the chiral critical endpoint. *Phys. Lett.* **2010**, *B682*, 401–407. [[CrossRef](#)]
143. Costa, P.; Ruivo, M.C.; Kalinovsky, Yu.L. Pseudoscalar neutral mesons in hot and dense matter. *Phys. Lett.* **2003**, *B560*, 171–177. [[CrossRef](#)]
144. Schaefer, B.J.; Wagner, M. The three-flavor chiral phase structure in hot and dense QCD matter. *Phys. Rev.* **2009**, *D79*, 014018. [[CrossRef](#)]
145. Horvatic, D.; Klabucar, D.; Radzhabov, A.E. η and η' mesons in the Dyson-Schwinger approach at finite temperature. *Phys. Rev.* **2007**, *D76*, 096009. [[CrossRef](#)]
146. Lenaghan, J.T.; Rischke, D.H.; Schaffner-Bielich, J. Chiral symmetry restoration at nonzero temperature in the $SU(3)_r \times SU(3)_l$ linear sigma model. *Phys. Rev.* **2000**, *D62*, 085008. [[CrossRef](#)]
147. Schaffner-Bielich, J. Effective restoration of the $U_A(1)$ symmetry in the $SU(3)$ linear sigma model. *Phys. Rev. Lett.* **2000**, *84*, 3261. [[CrossRef](#)]
148. Costa, P.; Ruivo, M.C. Kaons and pions in strange matter. *Europhys. Lett.* **2002**, *60*, 356–362. [[CrossRef](#)]
149. Anticic, T.; Baatar, B.; Barna, D.; Bartke, J.; Betev, L.; Białkowska, H.; Blume, C.; Boimska, B.; Botje, M.; Bracinik, J.; et al. Search for the QCD critical point in nuclear collisions at the CERN SPS. *Phys. Rev.* **2010**, *C81*, 064907. [[CrossRef](#)]
150. Hatsuda, T.; Kunihiro, T.; Shimizu, H. Precursor of chiral symmetry restoration in the nuclear medium. *Phys. Rev. Lett.* **1999**, *82*, 2840–2843. [[CrossRef](#)]
151. Cleymans, J.; Oeschler, H.; Redlich, K.; Wheaton, S. Transition from baryonic to mesonic freeze-out. *Phys. Lett.* **2005**, *B615*, 50–54. [[CrossRef](#)]
152. Friesen, A.V.; Kalinovsky, Yu.L.; Toneev, V.D. Strange Matter and Kaon to Pion Ratio in $SU(3)$ PNJL Model. *arXiv* **2018**, arXiv:1808.04179.
153. Moreira, J.; Morais, J.; Hiller, B.; Osipov, A.A.; Blin, A.H. Thermodynamical properties of strongly interacting matter in a model with explicit chiral symmetry breaking interactions. *Phys. Rev.* **2018**, *D98*, 074010. [[CrossRef](#)]
154. Morais, J.; Hiller, B.; Osipov, A.A. A general framework to diagonalize vector-scalar and axial-vector-pseudoscalar transitions in the effective meson Lagrangian. *Phys. Lett.* **2017**, *B773*, 277–282. [[CrossRef](#)]

